Integration and Optimization of a Solar Collector Heat Pump System Model for Households in The Netherlands

Integration and Optimization of a Solar Collector Heat Pump System Model for Households in The Netherlands

Thesis report

by

David E. Martinez Aguilera

To obtain the degree of Master of Science at the Delft University of Technology. To be defended publicly on:

Thesis committee:	Ivan Gordon, Rudi Santbergen, Emanuele Zanetti, Zain Ul Abdin
Main Supervisor:	Rudi Santbergen
Daily Supervisor	Zain Ul Abdin
Project Duration	September 2023 - July 2024
Student number	5616476

Sustainable Energy Technology (SET)
TU Delft
July 16, 2024

Preface

It seems impossible to capture and reflect all the hours, trials and errors, debugging, and small successes that have gone into researching this project over the past few months. Nonetheless, I will try my best.

First, I would like to personally thank my supervisors, Zain Ul Abdin and Rudi Santbergen, who provided valuable advice and guidance on the development of this project. I also extend my gratitude to my partners in the thermal group: Aron Van Rossum, Jaap Dijkstra, and Divye Kanawala. Each one of us put a lot of hard work into our thesis projects, but in some way, we gave a helping hand to each other. Lastly, and most importantly, I want to emphasize the significance of my family and friends, who have always been there for me.

David Martínez

Student Number: 5616476

Abstract

Photovoltaic-Thermal (PVT) modules, alongside Solar Thermal (ST) and Photovoltaic (PV) technologies, offer solutions to energy demands such as electrical consumption, space heating, and domestic hot water of residential buildings. This research employs a model-based approach to analyze how building insulation, solar collector configurations, and seasonal heating modes impact system design. Enhanced insulation scenarios demonstrate potential space heating demand reductions up to 70%, highlighting the relevance of proper insulation selection. The findings identify that using a PVT/PV configuration with one module per string is optimal, reducing roof area usage while achieving balanced thermal and electrical energy exchange. The analysis further reveals that higher indoor temperature settings substantially increase heating demands, suggesting significant energy savings potential through temperature set point adjustments. Operational heat supply strategies are adapted to seasonal variations, optimizing the use of solar energy and effectively incorporating aquifer thermal energy storage (ATES) systems as seasonal storage for winter months. But notably, the integration of PVT modules with heat pumps emerged as the primary driver of heat supply, contributing approximately 67% of the total heat demand.

Contents

List of Figures

List of Symbols

Greek Symbols

σ Stefan-Boltzmann Constant. [Watts per square meter per kelvin to fourth power]

α Heat transfer coefficient. [Watts per Celsius per square meter]

ϵ Surface emissivity. [-]

λ Thermal conductivity constant. [Watts per meter per Kelvin]

ρ Density. [Kilograms per cubic meter]]

η Efficiency. [-]

Latin Symbols

$\overline{W}_{Ap}$ Average power consumption of appliance i. [Watts]

a Absorption coefficient. [-]

F_{wwi} View factor from window to wall i. [-]

L Daily electrical load profile. [Watts]

Q_{per} Average heat produced by the standard person. [Watts]

ran Random value between 0 and 1. [-]

SLP Standard load profile. [Watts]

t Time [Hours]

ACH Air changes per hour. [Per hour]

f Appliance frequency of use [Per day]

N_p Maximum number of occupants in the household. [-]

$P_{\mathbf{H}}$ Hourly probability factor. [Day per hour]

$P_{\mathbf{Sea}}$ Seasonal probability factor. [-]

$P_{\mathbf{So}}$ Social probability factor. [-]

Q_H Heat production by occupants in the household. [Watts]

V_p Required ventilation mass flow per number of occupants. [Kilograms per second]

A_F Total household floor area. [Square meters]

DHW Domestic hot water in the household. [Kilograms per second]

F_{ij} View factor from surface i to surface j. [-]

h Enthalpy. [Joule per kilogram]

$P_{\mathbf{Acc}}$ Accumulative probability of turning on an appliance. [Per hour]

Q_{Heat} Space heating supply. [Watts]

Q_{Inf} Heat exchanged by infiltration. [Watts]

Q_{int} Household internal heat production. [Watts]

Q_{Ven} Heat exchanged by ventilation. [Watts]

r Heat pump variability with respect to the mean. [-]

R_{ins} Insulation thermal resistance of the household. [Square meters Kelvin per watts]

T_{Ave} Average temperature between surface i and surface j. [Celsius]

T_{cond} Condenser temperature jump. [Celsius]

T_{iw} Temperature of the inside wall node next to the surface node i. [Kelvin]

T^t_{iw} Temperature of the internal node closest to the outside concrete wall surface i. [Kelvin]

T^t_{oi} Outside concrete wall temperature in surface node i. [Kelvin]

T_{Sink} Heat pump sink temperature. [Celsius]

$\dot{m}$ Mass flow rate. [Kilograms per second]

G Total irradiance received by a surface. [Watts per square meter]

Q Heat. [Watts]

T Temperature. [Kelvin]

T_{Amb} Ambient temperature. [Celsius]

Subscripts and Superscripts

Air Related to the air properties.

$conv$ Convection.

DHW Related to the domestic hot water.

Gl Related to the window glass.

HP Related to the heat pump conditions.

i Related to the node i.

j Related to the node j.

rad Radiation.

$Room$ Related to the household/apartment.

S/i Surface of node i.

t Related to the instant t.

E Related to the electrical production or consumption.

Out Outlet conditions of the system or components.

PVT Related to the PVT module conditions.

$Ther$ Related to the thermal conditions of a component or system.

$Water$ Related to the properties of the water.

In Inlet conditions of the system or components.

Chapter 1

Background

One of the main energy goals in today's society is the reduction of fossil fuel usage, due to the increase in the atmosphere's CO_2 concentration over the past centuries. However, to achieve that goal another energy source should be both technically or economically feasible to scale it up. The good news is that solar energy generation releases zero CO_2 emissions during operation, and nowadays, these technologies are cheaper than fossil fuels in some applications such as electricity generation. Photovoltaic modules (PV) have been the most successfully deployed solar technology in the market. This technology has been used in both large-scale power plants and small household systems, covering a significant share of residential, commercial, and industrial electricity demands.

Over the last decades, solar energy technologies moved from research to market deployment. These technologies successfully have taken place in the electricity market. Figure 1.1a shows the evolution of installed photovoltaic power around the world. From 2006 to 2022, installed PV around the world increased by around 12,000%. In the case of The Netherlands, the total PV power increased by 2700% from 2013 to 2022, as indicated in 1.1b. Also, Figure 1.1a depicts the increase in PV roof power. This increase in PV roofs has been driven by net metering policies in the Netherlands.

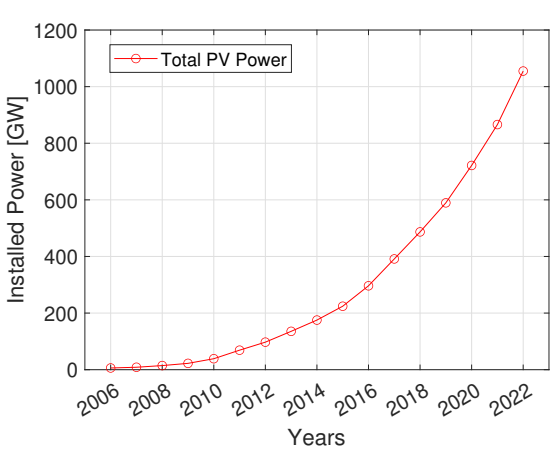

(a) Total PV power installed in the World.

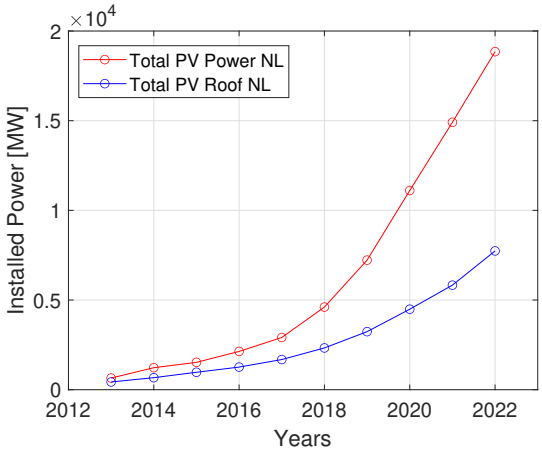

(b) Total PV power installed in the Netherlands.

Figure 1.1: Overview of PV solar production and installation trends. (a) Total PV power installed in the World. (International Renewable Energy Agency (IRENA), 2023) (International Renewable Energy Agency (IRENA), 2015) (b) Total PV power and PV roof power installed in the Netherlands. (International Renewable Energy Agency (IRENA), 2023) (Statistics Netherlands (CBS), 2022)

The net metering policy provides benefits to PV owners, which consists of giving the same value to the electricity produced by the PV installation and the one taken from the grid. In this way, PV installations that produce energy surplus into the grid will reduced their household's electricity bills. Even though net metering promotes PV installations, there are still some issues, because in this way residential PV owners evade paying transmission and distribution costs, which leads to users without PV, paying a higher tariff to cover the difference. (Cohen & Khermouch, 2013)

1.1 Background in residential energy sector

Energy in the residential sector can be expressed as heat or electricity. In both cases, consumption profiles are time-dependent due to weather conditions or consumer behaviors. Heat consumption is relevant in countries with cold weather seasons, due to the necessity of achieving comfortable temperatures inside buildings and houses. Meanwhile, electricity consumption is directly related to various consumer activities, including lighting, computer use, and the operation of household appliances.

Residential consumption contributes significantly to the final energy consumption in many countries. Figure 1.2a and Figure 1.2b show the evolution of each consumption sector in both the Netherlands and the world, respectively. In both situations, residential energy consumption has a similar share as other high energy consumption sectors such as Transport. However, while the annual residential consumption has remained stable over the last thirty years, this stability is not reflected at the individual level.

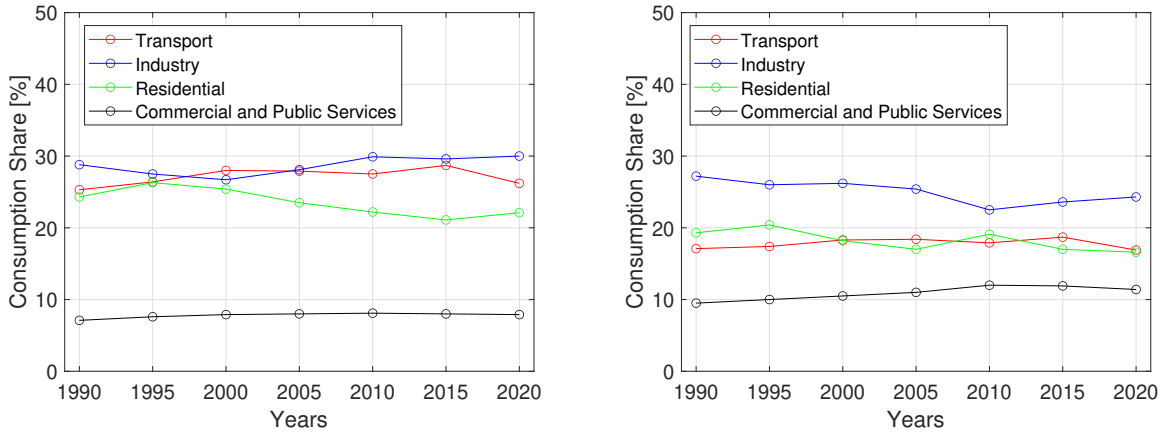

(a) World energy consumption share.

(b) The Netherlands energy consumption share.

Figure 1.2: Energy consumption share: Global vs. Netherlands (a) Consumption energy share in the world (b) Consumption energy share in the Netherlands. (International Energy Agency (IEA), 2022)

Household energy demand prediction depends on several factors such as occupant behavior and building characteristics. Occupant behavior is intrinsic to the type of occupant on the property. Several aspects had been considered relevant in the literature, such as family size (Fong, Matsumoto, Lun, & Kimura, 2007), age of occupants (York, 2007), and occupant energy savings tendency (Aydin, Kok, & Brounen, 2017). Meanwhile, building characteristics depend on the building properties and location, such as household size (Kowsari & Zerriffi, 2011), age of the building (Belaïd, 2016), population density in the surroundings (Porse, Derenski, Gustafson, Elizabeth, & Pincetl, 2016), number of cooling and heating days (Wiedenhofer, Lenzen, & Steinberger, 2013), wind speed (Sanaieian, Tenpierik, Van Den Linden, Seraj, & Shemrani, 2014), land surface temperature (Azevedo, Chapman, & Muller, 2016), and several other considerations. This situation suggests that obtaining a representative household demand curve may not be straightforward.

By analyzing several profiles of occupants, it resulted clear that low energy consumption occupants could led a building to reach net zero emissions with the proper building design (Carpino, Mora, Arcuri, & De Simone, 2017) (Barthelmes, Becchio, & Corgnati, 2016). However, for the same net zero emissions building a high energy consumption occupant consumes more energy than the produced in the building. This suggests that in energy-efficient buildings, occupant behaviors perform a primary role in the building design. Meanwhile, the effect of occupancy behavior and building characteristics for space and hot water heating in Dutch residential stock explains around 4.2% and 42% of total energy use, respectively (Santin, Itard, & Visscher, 2009). This analysis was done over old houses that could be considered non-energy efficient.

Occupant behavior models present a classification that accounts for each model complexity which are divided into four types (D'oca, Fabi, Corgnati, & Andersen, 2014). Type 0 uses non-probabilistic models that are based on derived schedules. Type 1 includes probabilistic models with methods such as Poisson processes or Markov chain. Type 2 increases the complexity of the models with object-oriented and agent-based models. The most common models are Markov chains, Bernoulli, and survival models. Markov chains consist of trying to predict the next time-step events based on current time-step conditions. In this way, behaviors such as switching on lights while entering a building space have a high probability. Bernoulli's models are concerned with the system component's state instead of the proper human-building interaction. However, theoretically, both systems lead to the same energy consumption. Meanwhile, survival models are statistical models that estimate the time until an event occurs such as how much time will pass until the occupant goes for lunch (Gilani & O'Brien, 2018).

Usually, in industry and academia, household consumption tends to be simplified with a standard load profile. However, using standard load profiles could underestimate the energy consumption in a household because standard load profiles typically are based on historical data and lack the latest updates in consumption behavior and technological trends (Hayn, Bertsch, & Fichtner, 2014).

Household energy demand models

Load curve modeling is classified into two approaches: top-down methods and bottom-up methods. Top-down methods are not concerned about the end-users energy consumption, those methods only consider the macroeconomic variables for the residential energy sector. Meanwhile, bottom-up methods construct the load curve by extrapolating the energy consumption of individual homes. Several bottom-up methods describe different consumption archetype trends that reflect several types of occupant behavior (Swan & Ugursal, 2009).

Usually, household bottom-up methods can be classified into statistical models and engineering method models. Statistical models are constructed with the energy bill information of energy suppliers to regress energy consumption considering household characteristics. Meanwhile, engineering methods can generate a consumption profile without any historical data by using physical models to estimate end-users consumption (Swan & Ugursal, 2009).

Household energy consumption

Household heating can be used either for maintaining comfortable temperature conditions as space heating (SH) or for occupant use as domestic hot water (DHW). Historically, natural gas is the primary energy source for heating, with consumption shown in Figure 1.3a. Figure 1.3a reflects the average gas consumption for different types of houses in the Netherlands. It is observable that larger house types tend to have higher heating consumption, which can be attributed to their greater wall surface area in contact with the environment. In the opposite case, apartments which are usually the smallest house type with less wall surface exposure, consume the least amount of heat on average. Additionally, Figure 1.3a indicates that all house types exhibit similar patterns of increase and decrease in gas consumption, likely due to annual weather variations.

Figure 1.4 shows the average annual electricity consumption of several household types. Similar to the case of heat consumption, traditionally smaller households consume less electricity than bigger ones, such as in the case of apartments and detached houses. Additionally, Figure 1.1a reveals that over the last decade, electricity consumption had a decreasing tendency, which could be explained by the use of new and more efficient equipment. This tendency dissolved in 2020, possibly due to COVID-19 lockdowns, which led to increased energy consumption as people were unable to leave their households.

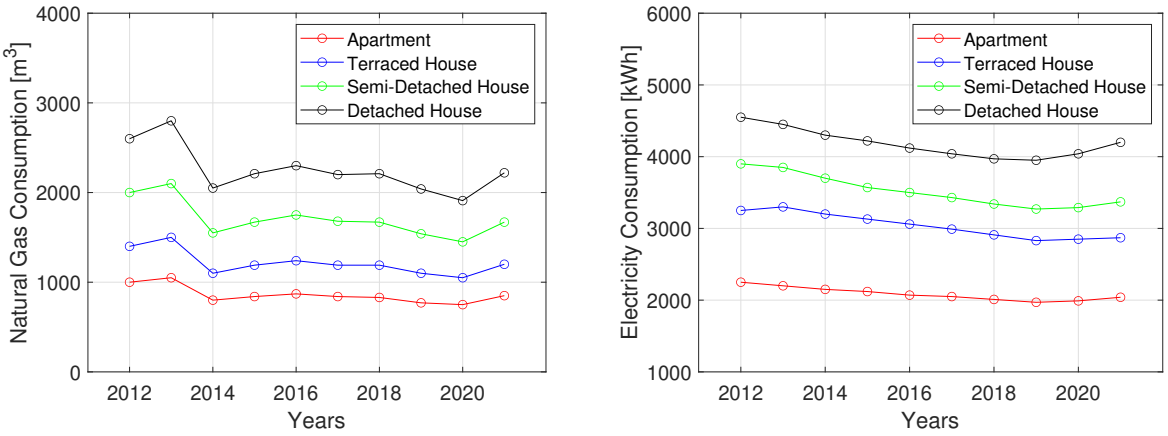

(a) Average natural gas consumption for several house types in the Netherlands.

(b) Average electricity consumption for several house types in the Netherlands.

Figure 1.3: Average energy consumption for various house types in The Netherlands: natural gas and electricity: (a) Average natural gas consumption for several house types in the Netherlands. (b) Average electricity consumption for several house types in the Netherlands. (Statistics Netherlands CBS, 2022b)

Power grids in the Netherlands are historically fossil-based. This can be seen from Figure 1.4, where in the last decades the Netherlands's power grid was mainly dependent on coal and natural gas. However, this dependence has been reduced by introducing non-fossil fuel sources like PV, wind, nuclear, and biomass. Even though, to this day, the power system is still primarily fulfilled using fossil fuel sources, this share has gradually been diminished over the past few decades. As illustrated by Table 1.1, in 2017, 85.9% of the total supply for the heating systems used in households came from natural gas. Meanwhile, other sources contribute on a much lower scale as solar heat with 0.6%, electricity with 2.8%, and heat pumps with 1.6%. This shows that the heat supply for households in the Netherlands is dominantly dependent on fossil fuels while renewable contribution is small.

Table 1.1: Energy sources consumption and contribution for household heating in the Netherlands. (Segers et al., 2019)

Energy Source	Consumption (PJ)	Contribution (%)
Natural gas	274	85.9
Oil	2	0.6
Solar heat	1	0.3
Biomass	16	5.0
Purchased heat	12	3.8
Electricity	9	2.8
Heat from environment by heat pumps	5	1.6

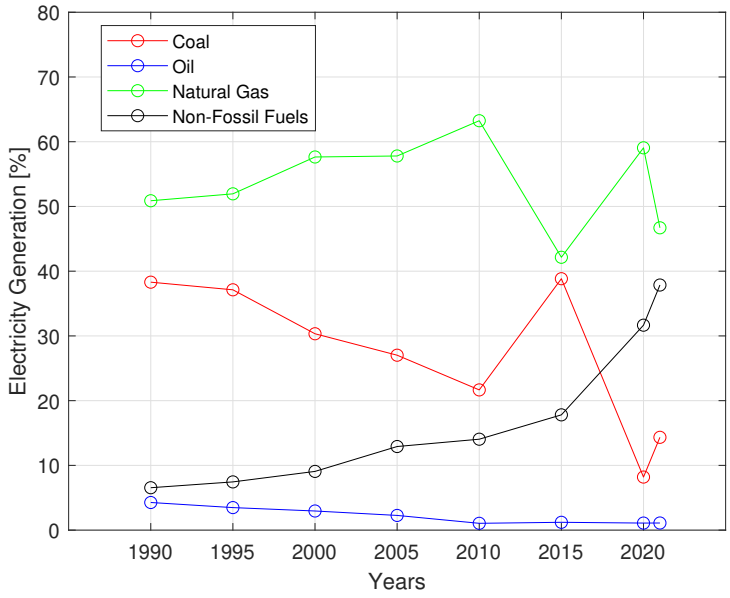

Figure 1.4: Electricity generation by source in the Netherlands. (Statistics Netherlands CBS, 2022a)

1.2 Solar technologies for residential application

The increasing electricity and gas prices have been a remarkable driver in the search for other methods and technologies to supply the household's energy demands. In this case, the Harmonized Index of Consumer Prices (HICP) for Energy is an index that measures the fluctuations in household energy prices. Figure 1.5 indicates a consistent increase of the HICP over the last 30 years, excluding the peak in 2022 due to the unforeseen Russia-Ukraine war. This trend motivates the development and use of new technologies to achieve self-consumption, such as solar technologies.

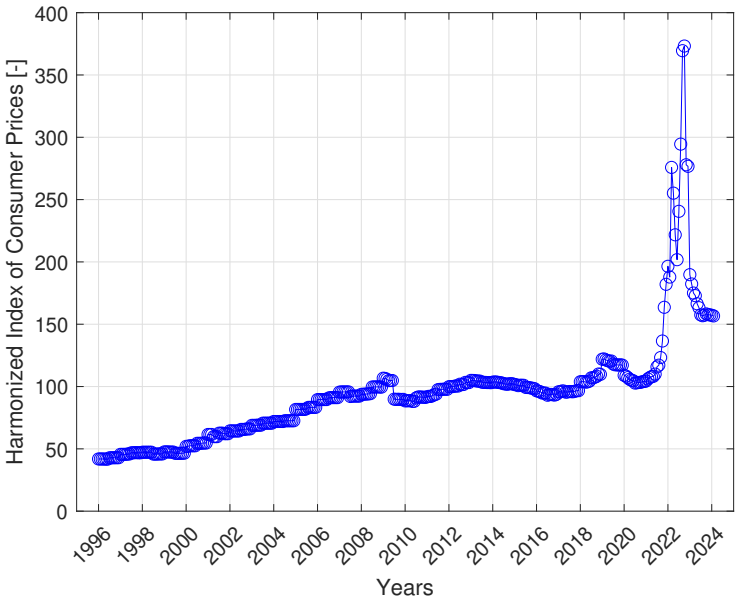

Figure 1.5: Harmonized Index of Consumer Prices: Electricity, Gas, Solid Fuels and Heat Energy for The Netherlands. (Eurostat, n.d.)

PV modules

PV modules are a technology that uses semiconductors and the photovoltaic effect to generate electricity by capturing solar irradiance. Single crystalline silicon is the most widely deployed PV technology in the market, with a maximum theoretical efficiency of 29.43% under standard test conditions (Richter, Hermle, & Glunz, 2013). However, under industry standards, a typical module efficiency of 20% is usually achieved with this material. Alternative options, such as thin-film technologies, but this type of modules experience lower efficiencies compared with single crystalline silicon modules (Benda & Černá, 2020).

The recent decrease in PV module prices has significantly driven the widespread implementation of PV systems. Between 2010 and 2020, the system cost dropped from 7.53 to 2.71 USD per installed Watt as shown in Figure 1.6. Figure 1.6 summarizes the cost evolution of residential PV systems during this period, highlighting that PV module costs were the primary cost factor for the entire system. This trend has reduced the simple payback period for a typical 4 kWp PV roof system to less than 11 years in several European countries, including France and Germany. However, in the Netherlands, the payback period was estimated to be between 11 and 14 years (Martinopoulos, 2020).

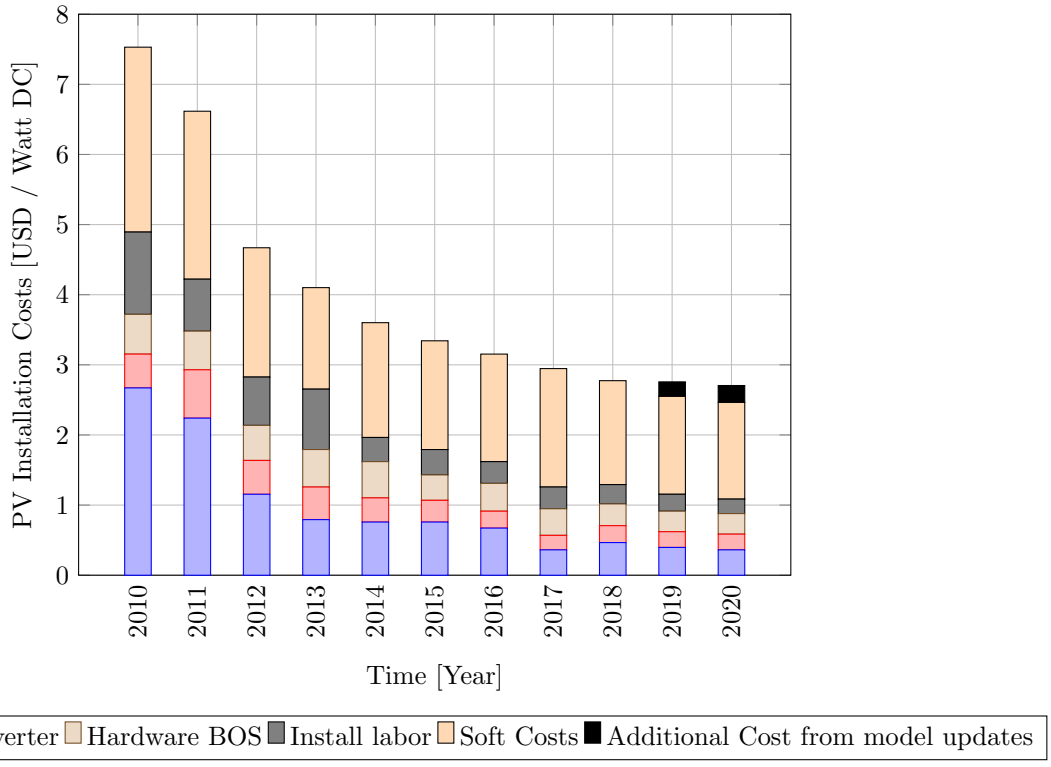

Figure 1.6: NREL Residential PV benchmark summary (inflation-adjusted), 2010–2020 (Feldman et al., 2021)

Solar thermal collectors

Solar thermal collectors (ST) utilize a broader solar spectrum range to generate heat, compared with the PV module's electricity production. The concept behind this process is that an absorbent material converts the incoming irradiance into thermal energy by increasing its temperature, which later is transferred into a working fluid to supply the heat demand. Solar thermal collectors on the market are classified as Evacuated tube collectors and Flat plate collectors. Evacuated tube collectors consist of a glass tube from which air is evacuated to minimize convection losses. Meanwhile, Flat plate collectors possess a simplified flat configura-

tion that only uses metallic absorbers in an encapsulated metallic plate (Ahmad, Khordehgah, Malinauskaite, & Jouhara, 2020).

For residential applications, currently, solar collectors are used due to the possibility of obtaining a low-temperature source of 60 C° for domestic hot water (Ahmadi et al., 2021). Solar thermal collectors have been used in countries with low temperatures, such as Canada, for various house types due to the significant heat production. However, some heat supply limitations appear during the winter season (Ampatzi, Knight, & Wiltshire, 2013).

Photovoltaic-Thermal modules

Photovoltaic Thermal (PVT) modules offer simultaneous production of both electricity and heat. This characteristic sets PVT modules apart from PV and ST technologies, which are limited to producing either electricity or heat individually. A PVT module consists of a PV module that produces electricity as any other PV module. However, a working fluid extracts part of the thermal energy that is produced by the PV module during operation.

The working fluid produces a cooling effect that influences the electrical efficiency of the PV cell in function of the mass flow rate and the inlet temperature (Herrando, Markides, & Hellgardt, 2014). At high flow rates, a lot of heat is extracted by the working fluid, providing a cooling effect that improves the electrical production from the PVT. But as shown in Figure 1.7a, even though the electrical efficiency improves while running high mass flow rates, the system's electrical efficiency decreases due to the electrical consumption of pumping the working fluid. However, contemporary PVT modules exhibit a reduced electrical efficiency (17.4%) when contrasted with the state-of-the-art efficiency of PV modules (20%) (Good, Andresen, & Hestnes, 2015).

In terms of thermal efficiency, using small mass flow rates allows for the extraction of only a small amount of heat, on the other hand, high outlet temperatures could be reached. But, by increasing the mass flow rate, the outlet temperature decreases but a higher heat amount could be extracted, as shown in Figure 1.7a. Meanwhile, Figure 1.7b highlights the impact of both PVT module insulation and the inlet temperature of the working fluid on thermal efficiency. When the inlet temperature of the working fluid is close to the ambient temperature, thermal efficiency improves. However, at higher inlet temperatures, thermal efficiency decreases because the working fluid's capacity to absorb the thermal energy of the PV module is reduced.

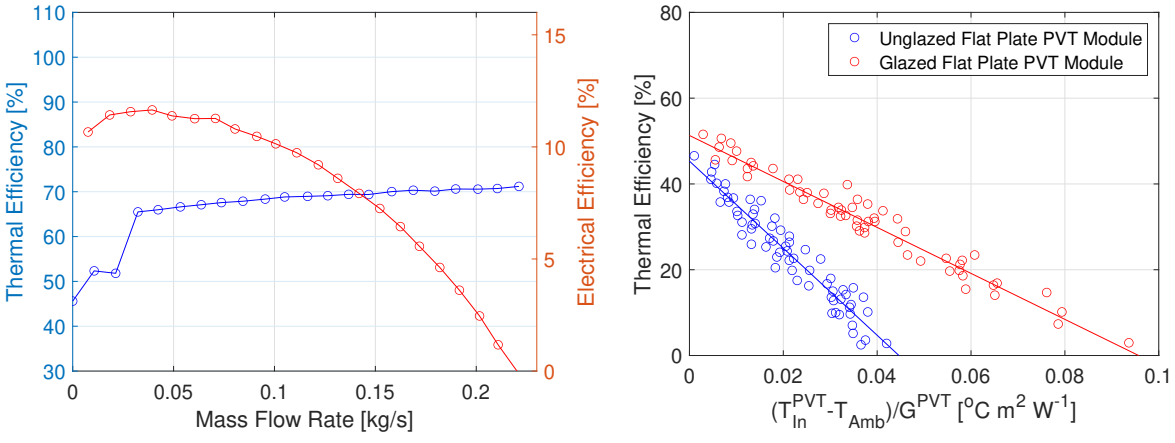

(a) Experimental PVT system efficiencies.

(b) Experimental PVT thermal efficiency.

Figure 1.7: Experimental PVT System Thermal Efficiency: Influence of Mass Flow Rate and Reduced Temperature: (a) Experimental PVT system efficiencies in function of flow rate. (Khani et al., 2019) (b) Experimental PVT thermal efficiency in function of the reduced temperature. (Kim et al., 2012)

The current market of PVT modules presents mainly three types of PVT: air-based (PVT/a), water-based (PVT/w), and solar-concentrated. Between those options, solar-concentrated doesn't have a market share compared to the other options. Meanwhile, water-based modules can achieve higher electrical and thermal outputs than other module types. Also, while comparing module costs, water-based PVT has mostly lower prices (Herrando et al., 2023).

Air-based models use air to draw heat from photovoltaic (PV) modules. This heated air can be utilized for ventilation, heating spaces, or drying. The most common type of air-based module is the flat-plate collector, which is effective for building applications in medium and high-altitude areas (Herrando et al., 2023). In regions with good solar energy and favorable temperatures, PVT/w systems can be used for heating spaces in winter and extracting heat from the air in summer, with the possibility of integrating heat pumps (Chow, 2018).

Heat pumps

A heat pump (HP) operates by using a working fluid to absorb heat from a low-temperature source, such as PVT modules or a geothermal reservoir, and transferring it to a high-temperature sink. Heat pumps can enhance the self-consumption of a PV system by converting excess electrical energy into thermal energy for storage (Williams, Binder, & Kelm, 2012).

Currently, there are three types of heat pumps on the market: air-source heat pumps, water-source heat pumps, and ground-source heat pumps. The primary difference between them is the heat source. PV air-source heat pumps are the most attractive investment for electricity prices below 0.23 €/kWh (Bellos, Tzivanidis, Moschos, & Antonopoulos, 2016). For higher electricity prices, PVT systems coupled with water-source heat pumps offer the best solutions.

ATES system

Typically, a mismatch occurs between solar production and residential energy consumption, leading to either an electrical or thermal mismatch. Solar production typically peaks around midday, while residential energy demand tends to be highest early in the morning or during the night. Therefore, energy storage is necessary to achieve self-consumption, allowing homeowners to utilize the energy generated by their solar systems.

To address this issue, surplus electricity can be fed back into the electrical grid or stored in batteries. In the case of heat storage, water storage heating tanks are the prevailing technology for residential applications, but their capacity is limited to a few days of heat capacity. Therefore, a long-term heat storage option is needed. One possible technology is the Aquifer Thermal Energy Storage (ATES) system, which stores heat in underground aquifers during peak summer when there is a surplus of heat production. This stored heat can then be used in the winter when there is no sun available for local heat production with solar technologies (Bloemendal, Jaxa-Rozen, & Olsthoorn, 2018).

1.3 Solar collector systems for households

Numerous studies have confirmed the economic viability of PV systems with heat pumps for residential buildings. A key factor in the economic viability of these systems is proper optimization, which can have a more significant impact on cost reduction than advanced control strategies (Angenendt, Zurmühlen, Rücker, Axelsen, & Sauer, 2019).

In contrast to PV systems, PVT technology is a relatively recent addition to the market, and fewer studies have been conducted on its residential applications. However, recent studies have shown promising results, indicating that PVT systems could meet a significant portion of household heating demand. For example, a study in Denmark demonstrated that a PVT system significantly reduced electricity and heat consumption compared to a house without the system

(Behzadi, Arabkoohsar, & Yang, 2020). Additionally, a study in the UK estimated the payback period for a PVT heat pump residential system to be 14 years, which is less than the lifespan of the system components (Sifnaios, Jensen, Dannemand, & Dragsted, 2021).

In the context of system optimization, accurately representing inputs such as load profiles is essential for properly sizing the entire system. Several studies have emphasized the importance of temporal resolution in understanding the dynamics of electrical load and PV generation for residential PV sizing (Beck, Kondziella, Huard, & Bruckner, 2016). These studies indicate that the choice of temporal resolution plays a crucial role, having a greater impact on load profiles than on PV profiles. Additionally, factors such as base load and peak load significantly influence self-consumption and the required battery size for the system (Linssen, Stenzel, & Fleer, 2017). Importantly, Linssen advises against relying on standard load profiles, as they tend to produce overly optimistic sizing scenarios.

1.4 Literature gaps and improvements

A literature gap exists in optimizing household PVT systems, especially concerning occupant behavior and building characteristics impact on system sizing, particularly for thermally efficient houses. Furthermore, there is a need to explore the implication of using several heating modes that influence the overall sizing of all system components like PV, PVT, ST, heat pumps and thermal storage as ATES system.

For precise sizing of a PV/PVT system, a representative load profile estimation is essential. Relying only on standardized load profiles can result in an undersized system. Therefore, a more detailed approach is required, one that refines standard load profiles. Moreover, many parameters are interrelated with load profiles in PV system optimization. One feasible approach involves assigning probability to different appliances at various times of the day.

1.5 Research objective

The primary objective of this thesis is to quantify the technical feasibility of using PVT modules as the only energy source by simulating the heat supply in households or buildings. This involves integrating all components of the PVT-HP residential systems to optimize the number of solar collector modules required to meet the thermal and electrical demands of various household types. The following sub-objectives were established to accomplish the main objective:

- **Describe the system model integration methodology. (Chapter 2)**
  Present the chosen integration methodology to model the heat demand of a building, the heat and electricity supply from solar collectors, and the methods to meet these demands. This system model integration will account for seasonal and daily variability, by taking into account the technical requirements for proper heat supply.

- **Development and validation of the heat demand model together with system model integration. (Chapter 3)**
  Create and validate a space heat demand model, integrating it with each system component model. This will facilitate the analysis of different methods to meet household heat demands and optimize solar collector system sizing based on building characteristics.

- **Sensitivity analysis over the integrated system model. (Chapter 4)**
  Conduct a sensitivity analysis of the space heat demand model to assess the influence of building characteristics over solar collector sizing and configuration. This analysis will identify the most suitable configurations based on various building characteristics such as number of stories, type of insulation, and floor area.

- **System and viability analysis of using solar collectors on real buildings in Amsterdam. (Chapter 5)**
  By considering heat demand profiles for several residential buildings from the AMS Institute, an estimation is obtained of solar collector system size for residential buildings in Amsterdam. This analysis will determine the technical feasibility of supplying the heat demand while fitting the solar collectors in the roof area of those buildings.

Chapter 2

Methodology

The chosen methodology to build an integrated system capable of estimating the required PVT system sizing for several buildings is structured around three key components: model selection and construction, system model integration, and system analysis. First, the system models will be described, then the integration of each model with each other will be established, and finally, the system will be applied to several building cases.

Model construction involves developing a space heating demand model, a domestic hot water demand model, and an electrical consumption household demand model. These models are designed to be user-friendly for individuals without specialized knowledge in heat demand modeling, unlike conventional heat demand modeling software such as EnergyPlus™. This construction process considers relevant parameters, including household type and characteristics like floor area, façade details, and wall properties. Additionally, each household is associated with a specific number of occupants.

The system model integration process is depicted in Figure 2.1, where input data such as weather and location data, household characteristics, and occupant types are required either for energy production or energy consumption. These inputs collectively generate the electrical and heat demand profiles for each household, while determining the energy production from PV, PVT, or ST systems. This produced energy is then utilized to meet the demand through the utilization of the heat pump and an ATES system.

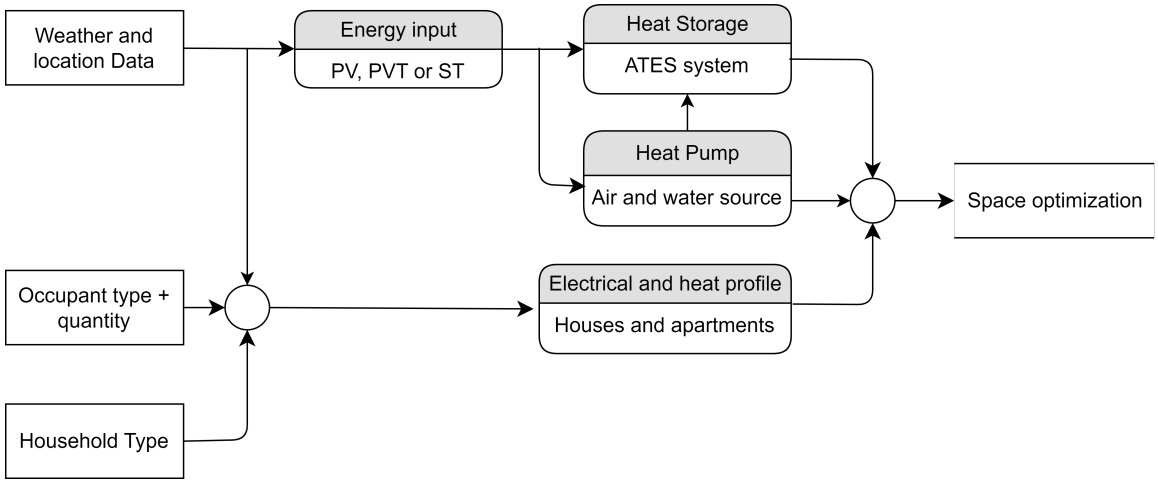

Figure 2.1: Solar collector heating system integration strategy for residential buildings.

The system analysis employs the integrated system to evaluate the impact of building characteristics over the solar collector system sizing, to then use it for real residential buildings in Amsterdam. This analysis allows for the determination of the necessary amount of PV, PVT, and ST modules to address thermal mismatches throughout the year under various conditions, facilitating the achievement of the main project objectives.

2.1 Models description

Irradiance model

The irradiance models incorporated into the PVMD Toolbox utilize the Perez model, Smarts, and ray tracing methodologies. The Perez model is an extension of the CIE standard clear sky formula (International Commission on Illumination (CIE), 1973), employing five parameters to accurately depict a wide range of luminance distributions—from clear sky scenarios to complete overcast conditions (Perez, Seals, & Michalsky, 1993). Concurrently, the SMARTS model is a spectral radiation model, that calculates solar shortwave direct beam irradiance in cloudless atmospheres. It considers atmospheric processes such as Rayleigh scattering, aerosol extinction, and absorption by ozone, gases, water vapor, and nitrogen dioxide. Notably, the SMARTS model has exhibited enhanced accuracy, particularly in the UV, validated through comparisons with rigorous radiative transfer models and measured datasets (Gueymard et al., 1995). By integrating all three models, the PVMD Toolbox delivers a detailed irradiance assessment for each cell module.

PV model

The PVMD Toolbox employs a fluid dynamic model to approximate temperature variations during the operation of a photovoltaic module under varying irradiance conditions. This is achieved through an energy balance applied to the PV module, treating it as a homogeneous mass with a consistent temperature. The module undergoes heat influx in the form of irradiance, which is not converted into electricity, and dissipates heat through convection to the surrounding ambient temperature, as well as radiation to the sky and ground. Within this model, the convective heat transfer parameter is characterized using empirical data dependent on different wind speeds. This empirical data is then compared with predictions from established models, ensuring the accuracy and reliability of the convective heat transfer parameter in the overall estimation of temperature changes during PV module operation (Fuentes, 1987).

In the electrical simulation for PV modules, the one-diode model is applied. This involves employing a lumped-element model to simulate the module's interconnection with bypass diodes, enabling the computation of module IV curves for every hour of the year. The initial step entails calculating time-resolved IV curves for each cell. To achieve this, the input parameters include I-V curves, photocurrent, and module temperature (Vogt et al., 2022).

PVT and ST module

In contrast to the PV model, both PVT and ST modules are estimated through the models proposed by Ul-Abdin (Ul-Abdin, Zeman, Isabella, & Santbergen, 2024). These equations estimate both thermal and electric efficiency through Equation 2.1 and Equation 2.2, by incorporating the inlet working fluid temperature (T_i) and ambient temperature (T_{amb}) under several possible irradiances. This model describes the behavior of a PVT and ST module (either air-based or water-based) by fitting real-life data or a highly detailed model data from the PVMD Toolbox, into the parameters a_1, a_2, b_1 considering the standard thermal and electrical efficiencies, $\eta_{Ther}(0)$ and $\eta_E(0)$, respectively.

$$\eta_{Ther}^{PVT} = \eta_{Ther}^{PVT}(0) - a_1 \frac{T_{In}^{PVT} - T_{amb}}{G^{PVT}} - a_2 \Big(\frac{T_{In}^{PVT} - T_{amb}}{G^{PVT}} \Big)^2 \tag{2.1}$$

$$\eta_E^{PVT} = \eta_E^{PVT}(0) - b_1 \frac{T_{In}^{PVT} - T_{amb}}{G^{PVT}} \tag{2.2}$$

Then, by utilizing the module's efficiencies, the instantaneous thermal power (Q_{Ther}^{PVT}) and electrical power (Q_E^{PVT}) generated by the PVT module can be calculated using Equation 2.3 and Equation 2.4. By taking into account the heat produced from the PVT module or the ST module, the temperature rise in the working fluid passing through it can be estimated, leading to an approximation of the outlet working fluid temperature through Equation 2.5.

$$Q_{Ther}^{PVT} = \eta_{Ther}^{PVT} \cdot A^{PVT} \cdot G^{PVT} \tag{2.3}$$

$$Q_E^{PVT} = \eta_E^{PVT} \cdot A^{PVT} \cdot G^{PVT} \tag{2.4}$$

$$T_{Out}^{PVT} = T_{In}^{PVT} + \frac{Q_{Ther}^{PVT}}{\dot{m}^{PVT} \cdot C_P^{Water}} \tag{2.5}$$

Aquifers thermal energy system

In seasonal storage modeling, a key parameter of interest is the heat balance between the energy extracted and injected into the storage system. This project employs a system utilizing two aquifers (one hot and one cold). The evolution of aquifer temperatures is estimated by considering the heat balances as outlined by Van Rossum in the PVMD Toolbox (van Rossum, 2024). This energy balance is necessary to maintain a constant average aquifer temperature throughout the year, as the heat exchanged with the aquifers should be close to zero.

Heat pump model

The PVMD Toolbox presents a heat pump model that uses a fitted COP equation to determine the amount of heat that is enhanced. But for the scope of this project, to accurately simulate the heat pump system, a thermodynamic cycle is utilized to improve the quantification of the heat transferred for both space heating and domestic hot water demands. The key components of the heat pump are depicted in Figure 2.2a, which is divided into evaporation (from D to A), compression (from A to B), condensation (from B to C), and expansion (from C to D) as indicated by Grassi (Grassi, 2017). Meanwhile, Figure 2.2b illustrates the thermodynamic cycle of the heat pump, starting at point D where a coolant absorbs heat in the evaporator. Instead of increasing its temperature, the coolant changes phase from liquid to gas through evaporation, reaching point A. Exiting the evaporator, the coolant in gaseous phase is compressed by a compressor, raising both pressure and temperature, culminating at point B. Subsequently, in the condenser, the coolant releases heat primarily condensing while exchanging heat until reaching point C. Finally, the fluid returns to point D through pressure reduction in an expansion valve, restoring the initial cycle conditions.

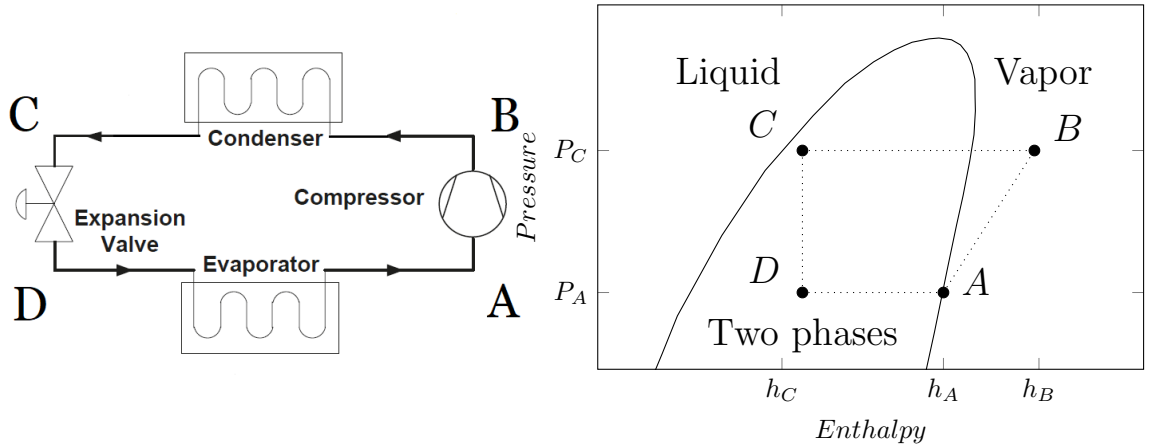

(a) Heat pump thermodynamic processes.

(b) Heat Pump Thermodynamic Cycle ($P-h$ curve)

Figure 2.2: Simplified heat pump diagram with the thermodynamic cycle representation.

The modeling applied in the thermodynamic cycle for Figure 2.2b shall be solved for each hour of the year, taking into account the fluctuating thermal conditions used for both space heating and domestic hot water as proposed by the cycle suggested by Chaturvedi et al. (Chaturvedi, Gagrani, & Abdel-Salam, 2014). The COP of the heat pump is determined by including these thermodynamic considerations in the current statistical data model. Including the thermodynamic considerations of Ruhnau et al. equations in the PVMD Toolbox (Ruhnau, Hirth, & Praktiknjo, 2019). The required sink temperature is then calculated according to Equation 2.7 which depend of the type of technology used according to Ruhnau et al. (Ruhnau et al., 2019)

$$T_C^{HP} = T_{Sink} + T_{cond} \tag{2.6}$$

$$T_{Sink} = \begin{cases} 30 - T_{Amb} & For\ radiators \\ 30 - \frac{1}{2}T_{Amb} & For\ floor\ heating \end{cases} \tag{2.7}$$

To solve the thermodynamic cycle for each hour, a constant evaporator temperature of 0 °C is considered (Yıldız & Yıldırım, 2021), and point A is assumed to be a saturated gas. To determine the enthalpy at points B and C, the COP definition is used along with a fitted COP equation described by Ruhnau et al. (Ruhnau et al., 2019). Here, T_{Sink} is the temperature needed for space heating or the radiator, while T_{Source} is the temperature of the water that provides heat to the heat pump. Additionally, ideal gas compression behavior is assumed, as indicated by Chaturvedi (Chaturvedi et al., 2014).

Household electrical demand and domestic hot water demand

To generate the household electrical demand and the domestic hot water demand load profile, a similar approach is used in both cases to model occupancy behavior. In the case of the electrical profile model comprises three key elements: a detailed list of appliances, occupancy behavior, and construction. The list of appliances catalogs all devices in the household, each requiring a representative curve. Simultaneously, the occupancy behavior model assigns a probability of use to each appliance for every hour of the day, allowing flexibility to explore various occupant profiles by adjusting parameters in the occupant behavior model. By integrating the occupant model with representative load curves for each appliance, an electrical load specific to a certain

type of occupant and house can be obtained. The occupant model must consider weekday and weekend variations.

The occupant behavior aligns with the methodology established by Paatero et al. (Paatero & Lund, 2006), where, for each time step, every appliance has a probability of activation. This probability is determined by factors including seasonal variation, routine use, social influences such as weekday and weekend variations, and the number of occupants. The mathematical expression for this approach is illustrated in Equation 2.8:

$$P_{\mathrm{Acc}} = P_{\mathrm{Sea}} \cdot P_{\mathrm{H}} \cdot f \cdot P_{\mathrm{So}} \tag{2.8}$$

Where:

- P_{Acc}: accumulative probability of turning on an appliance.
- P_{Sea}: seasonal factor, modeling seasonal changes.
- P_{H}: hourly probability factor, modeling activity levels during the day.
- P_{So}: social factor, modeling weather and social factors influencing communal behavior.
- f: mean daily starting frequency, modeling the mean frequency of appliance use.

For the heat load curve construction, factors such as transmission gains/losses, internal gains, infiltration/ventilation losses, and solar gains are considered. The occupant model plays a crucial role by providing information about the times when people are present in the household, influencing the heat load curve accordingly. This approach ensures a more accurate representation of energy consumption patterns.

2.2 System inputs

Weather data

To accurately represent irradiance and weather conditions, Meteonorm™ can be employed to obtain accurate weather data for a standard year at a chosen location. This process involves obtaining data on all irradiation components, temperatures, and wind speed conditions, all of which significantly impact the performance of solar modules and the amount of heat required in a household.

Building characteristics

An accurate definition of the main building's characteristics is necessary for determining the required heat that should be supplied to each household. To properly model each household a dynamic multi-nodal model is employed, in which the following heat modes are taken into account:

- Transmission Losses/Gains: A detailed consideration of the building's surface interaction with the surroundings is crucial for accurately estimating heat transfer, which is produced by the temperature difference between the indoor and outdoor environments.
- Solar Gains: Through each window, it's essential to account for the irradiance that contributes to the heat gain inside each dwelling, especially when considering the dynamic effects on indoor temperature.

- Internal Gains: Internal heat generation within dwellings comes from the operation of electrical appliances, which dissipate heat. In addition, the heat generated by occupants further influences the overall heat load that needs to be accommodated within the system.

- Advection (Ventilation + Infiltration): A continuous air mass flow at ambient conditions should be introduced into households (ventilation) to maintain air quality, alongside an involuntary air mass flow that infiltrates each household. Both mass flows affect the overall indoor temperature of the building, which should be taken into account.

2.3 System analysis and operational modes

For the system analysis, the main building characteristics and solar collector configurations are taken into account to evaluate their influence in sizing a system to minimize the usage of roof area. This includes main characteristics in terms of the type of houses: detached or mid-row, number of stories in each home, floor area per house, and indoor temperature for each dwelling. Such scenarios will influence the heat demand and consumption profile in the integrated system.

A representation of the system= is depicted in Figure 2.3, which delineates two subsystems: one dedicated to space heating and the other to domestic hot water. This differentiation is essential due to the difference between the final temperature requirements associated with each type of heat application. Additionally, from a technical standpoint, it is crucial to ensure that the ATES system and the solar collector do not share the same heat pump. This is because the fluid circuits of the PVT system and the ATES system operate independently, both in terms of time and spatial configuration. The ATES system connects to each building via underground pathways and typically operates during periods of high heat demand, such as in winter. Conversely, the heat pump for the PVT system must operate during the whole year.

By using separate heat pumps from the ATES and PVT systems, each heat pump can consistently operate at its nominal power during its designated operating periods. In contrast, utilizing a single heat pump for both systems would result in optimal performance only during winter, thereby limiting efficiency throughout the rest of the year.

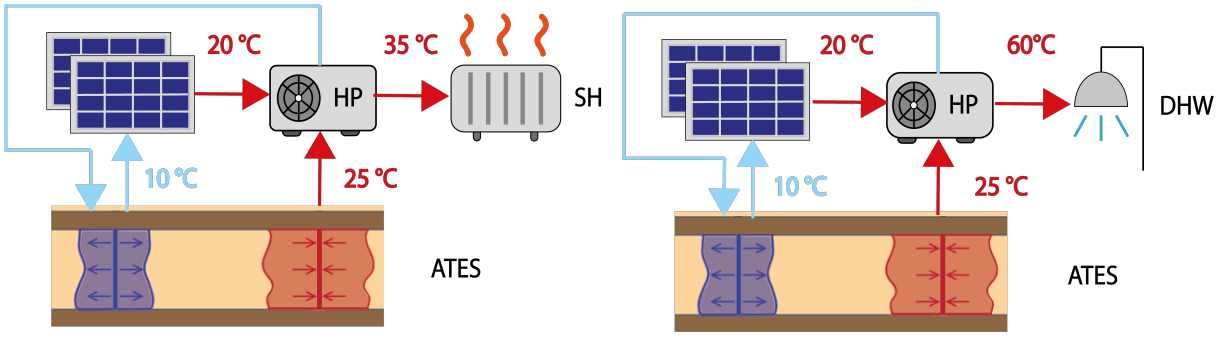

Figure 2.3: Schematics of the whole heating system, including the solar collectors, heat pump, ATES system, SH and DHW. [A separate HP is considered for the PVT system and the ATES system. However, for the sake of simplicity in the diagram, they are illustrated as utilizing the same heat pump.]

Meanwhile, the operational modes aim to fulfill the heat demand in each dwelling throughout the year, which relies on the weather dependency of solar energy. As illustrated in Figure 2.4, the system integrates a solar collector (PV, PVT, and/or ST) as an energy source, and seasonal heat storage in this case an ATES system. The heat collected should address DHW and SH requirements inside each dwelling at the respective temperature levels for each application by using or not a heat pump.

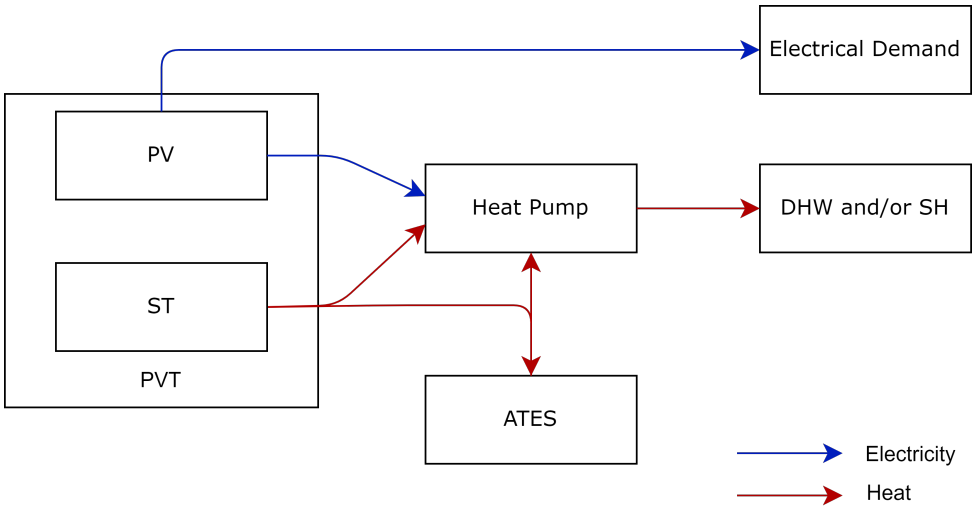

Figure 2.4: Schematics of the energy flows of the household heating system.

To accurately model this system, an energy balance throughout the year must be conducted. This is achieved by considering three operational modes that describe the interactions of heat production. The first mode, called "Summer mode" (or Mode 1), describes the primary heat production of the year that occurs during the summer months. In this mode, the heat is directly supplied to the DHW and/or SH systems without the use of a heat pump as shown in Figure 2.5a. Otherwise, when the heat demand is fulfilled or not needed, the residual heat, from Summer mode or any other operational mode, is stored in the ATES system as shown in Figure 2.5b.

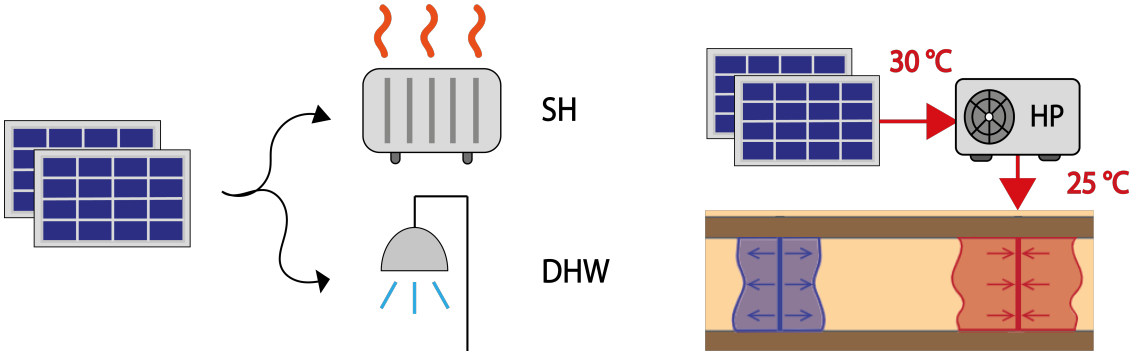

(a) Heat supply of summer mode.

(b) Storing excess heat into ATES system.

Figure 2.5: Representation of the Operational Mode 1, also called Summer Mode. (a) Heat production while the outlet temperature fulfills the temperature requirements of SH and DHW. (b) Excess heat stored in the ATES system by adjusting the temperature using a heat pump.

Meanwhile, during many hours of the year the output temperature of the solar collector system is considerably lower than the required temperature for either SH or DHW. In these situations, a heat pump is needed to achieve a sufficiently high temperature for SH and/or DHW. This operational mode is called "Spring mode" (or Mode 2). Spring mode operates for most of the year, particularly when heat can be extracted from the water of the solar collector system. This mode primarily provides heating during spring and autumn when the heat demand inside the houses is not as high as in winter, but still present. A representation of Spring mode is shown in Figure 2.6, noting that the heat pumps for SH and DHW should be different due to the differences between the output temperatures for each application.

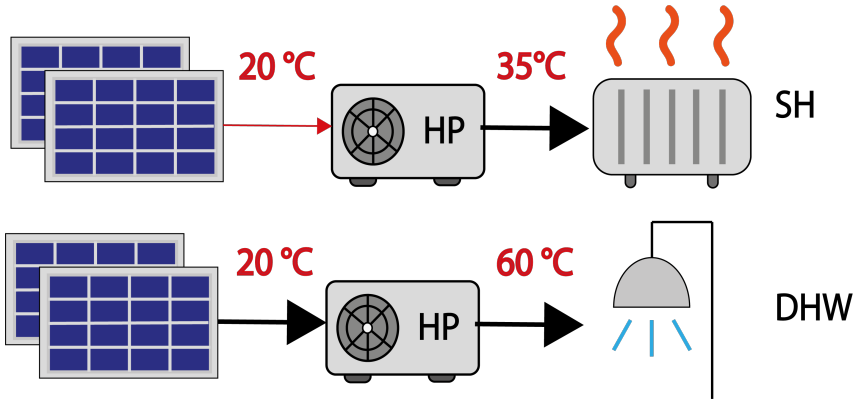

Figure 2.6: Representation of the Operational Mode 2, also called Spring Mode. Heat is produced by PVT modules or ST modules and then enhanced by the HP to supply SH or DHW.

For such conditions in which the heat demand cannot be fulfilled by summer mode and/or spring mode, "winter mode" (or Mode 3) is also there to play its role. This operational mode is conducted by the use of the heat stored from the seasonal heat ATES system to make up for the difference in the heat demands for the whole household. Winter mode is represented in Figure 2.7 in which a temperature increase is obtained by the use of a heat pump. It is important to remark that the ATES store heat seasonally, which means that surplus heat during summer should be store as illustrated in Figure 2.5b to then be used for winter mode.

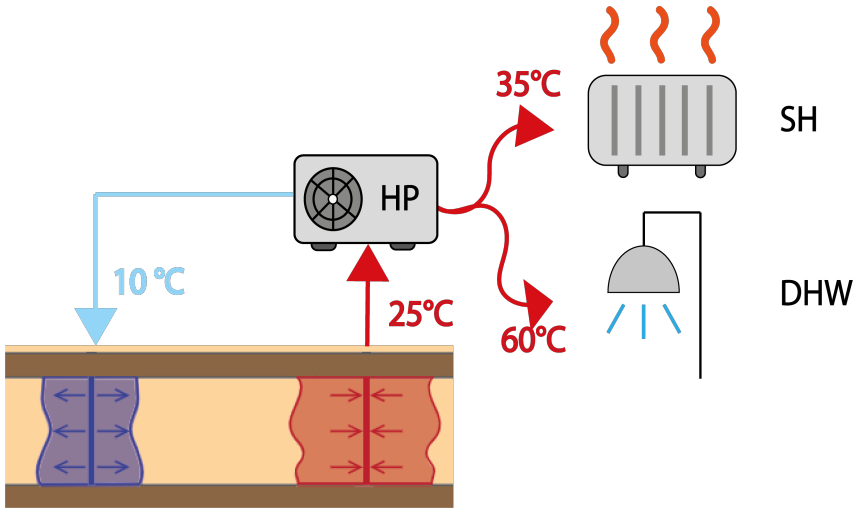

Figure 2.7: Representation of the Operational Mode 3, also called Winter Mode. Heat is extracted from the ATES system (hot aquifer) and then enhanced with a heat pump to supply the heating demand, and the cooled mass flow returns to the cold aquifer. (Duijff et al., 2023).

2.4 Conclusions

The project methodology focuses on three primary components: model construction, system integration, and system analysis. Model construction includes developing user-friendly models for space heating demand, domestic hot water demand, and household electrical consumption, utilizing various household data inputs. For system model integration, the project incorporates models from the PVMD Toolbox, such as PV, PVT, and heat pump models, to supply the electrical and heat demand for each household.

The system analysis phase evaluates the impact of various building characteristics on energy

demand and production. Factors such as floor size, number of stories, wall insulation, and indoor temperature are analyzed to determine the appropriate number of PV, PVT, and ST modules needed throughout the year. This analysis helps identify optimal configurations to address thermal mismatches.

Chapter 3

System Model Integration and Validation

3.1 Purpose of the space heating model

The model is designed to simplify the simulation of thermal demand within individual dwellings or clusters, as depicted in Figure 3.1, in which it is possible to model several types of houses. Unlike other programs such as EnergyPlus™, this model requires basic building characteristics, making it accessible to individuals without specialized knowledge in heat demand modeling and integrating it into the PVMD Toolbox. Notably, users have the flexibility to adjust the thermal properties of the household, facilitating simulations to various types of households, from those with low thermal insulation to well-insulated houses.

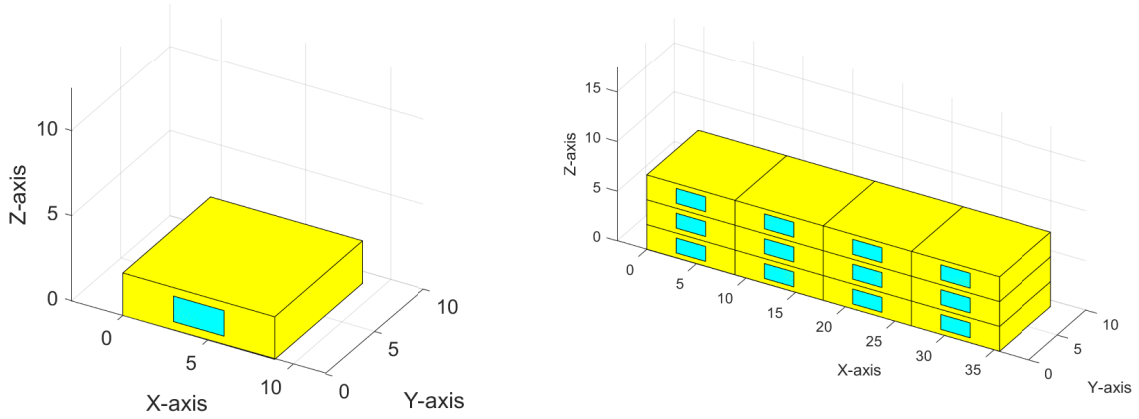

(a) Representation of a single house that can be modeled. (b) Representation of the apartment complex that can be modeled.

Figure 3.1: Representation of the types of buildings that can be modeled with the space heating model.

3.2 Space heating model

To accurately estimate the heat demand in a residential building, a space heating demand model is developed using a thermal resistance network. This model incorporates the dwelling's characteristics, including building geometry (assuming that each apartment consists of four walls and a window in its façade), together with their respective thermal properties and insulation. In this way, it becomes possible to determine the heating demand in each house/apartment by considering various transmission modes: convection, radiation, solar gains, internal heat production, and heat accumulation.

3.2.1 Convection

Equation 3.1 models the heat transfer by convection between the inside and outside walls of the house. By coupling a surface node temperature ($T_{S/i}$) with either room temperature or the outside temperature, depending on whether the surface wall is external or internal. In all the cases, the convection factor (α_{conv}) is taken to be constant and equal to 25 W/m^{2}K on the external surface and 5 W/m^{2}K on the internal surfaces (Bergman, Lavine, Incropera, & DeWitt, 2007).

$$Q_{conv} = \alpha_{conv} \cdot A_{S/i} \cdot (T_{Room} - T_{S/i}) \tag{3.1}$$

3.2.2 Radiation

To account for radiation heat exchange over the internal surfaces in each household, Equation 3.2 is utilized. In the model, the radiation heat transfer coefficient (α_{rad}) remains constant, primarily due to the uniformity of temperatures in the internal walls. This coefficient is expressed as a function of emissivity (ϵ), the Stefan-Boltzmann Constant (σ), and the average temperature T_{Ave} as shown in Equation 3.3. Given the small variations in indoor temperatures, the radiation heat transfer coefficient is considered constant (Bergman et al., 2007).

$$Q_{rad} = \alpha_{rad} \cdot A_{S/i} \cdot F_{AB} \cdot (T_{S/i} - T_{S/j}) \tag{3.2}$$

$$\alpha_{rad} = 4\epsilon \cdot \sigma \cdot T_{Ave}^3 \approx 5 \tag{3.3}$$

For calculating the view factor (F_{12}), the analytical solution applicable to perpendicular rectangles is utilized, as illustrated in 3.2. This approach fits the assumption that each dwelling is modeled as an empty box. The analytical equations corresponding to this assumption are illustrated in Equation 3.4, 3.6, 3.7, and 3.8.

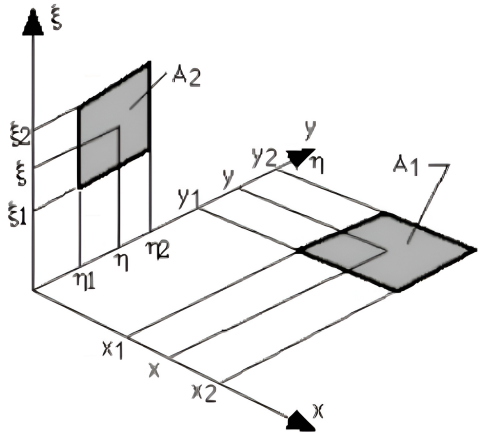

Figure 3.2: View factor description for two perpendicular rectangles, that represent the internal walls of each modelled apartment or household.

$$F_{12} = \frac{1}{2\pi A_1} \sum_{l=1}^{2} \sum_{k=1}^{2} \sum_{j=1}^{2} \sum_{i=1}^{2} \Big[(-1)^{i+j+k+l} \cdot B(x_i, y_j, \eta_k, \xi_l) \Big] \tag{3.4}$$

$$A_1 = (x_2 - x_1) \cdot (y_2 - y_1) \tag{3.5}$$

$$B = (y - \eta) \cdot C \cdot arctan(D) - \frac{C^2}{4} \cdot (1 - D^2) \cdot ln\Big[C^2 \cdot (1 + D^2)\Big] \tag{3.6}$$

$$C = \sqrt{x^2 + \xi^2} \tag{3.7}$$

$$D = \frac{(y - \eta)}{C} \tag{3.8}$$

3.2.3 Solar gains

Regarding solar gains, the heat absorbed by the window glazing is determined using Equation 3.9. This equation takes into account the absorption coefficient of the window glazing (a^{Gl}), the window area (A_{Gl}), and the irradiance (G_{Gl}) reaching the window to compute the absorbed irradiance by the glass (Q^{Gl}). Additionally, to account for solar irradiance reaching each surface inside the households, the view factor is employed to estimate the proportion of irradiance reaching the walls. Instead of utilizing the window absorption coefficient, the absorption coefficient of the concrete wall (a^{Con}) is applied, as indicated in Equation 3.10.

$$Q^{Gl} = a^{Gl} \cdot A_{Gl} \cdot G^{Gl} \tag{3.9}$$

$$Q^{Room} = a^{Con} \cdot F_{wwi} \cdot A_{Gl} \cdot G^{Gl} \tag{3.10}$$

3.2.4 Internal heat

In the case of internal heat, both electrical consumption and human heat production are estimated through an occupant behavior model. For electrical consumption, the established method is described in Subsection 2.1, where a detailed list of appliances is used to approximate an electrical load profile. This is illustrated in Equation 3.11, taking into account all typical electrical appliances in a household and their average consumption ($\overline{W}_{Ap}$).

$$L = \sum_{i=1}^{\#appli.} \overline{W}_{Ap} \cdot g(P_{Sea}(x,t), P_H(y_i), f_i, P_{So}) \tag{3.11}$$

In the construction of the electrical load profile, the consideration of a seasonal variation (P_{Sea}) is essential. This variation is modeled as a sinusoidal function, which represents the tendency for higher electrical consumption during winter and a decrease in consumption during summer, as expressed in Equation 3.12. Additionally, the probability of operation (P_H) quantifies the likelihood of an appliance running on a certain hour in a standard day within a household. This probability (y_i) is assigned to each appliance for every hour of the day.

$$P_{Sea} = 1 + x \cdot sin(\frac{2\pi t}{8760}) \tag{3.12}$$

$$P_H(t_i) = y_i \tag{3.13}$$

Through the daily appliance frequency of use (f_i) and the social factor of use (P_{So}), it is possible to describe the energy consumption deviation from the standard user through Equation 3.14. In this way, the operational conditions of each appliance are estimated for every hour of the day. But to do this, the accumulated probability is compared with a randomly generated value (σ_{ran}) ranging from 0 to 1. If the accumulated probability is higher than the randomly generated value the appliance is turned on, in the opposite case, the appliance is turned off.

$$g(P_{Sea}(x,t), P_H(t), f_i, P_{So}) = \begin{cases} 1 & \text{if } P_{Sea}(x,t) \cdot P_H(t) \cdot f_i \cdot P_{So} > ran \\ 0 & \text{if } P_{Sea}(x,t) \cdot P_H(t) \cdot f_i \cdot P_{So} < ran \end{cases} \tag{3.14}$$

Due to the difficulty of obtaining the daily consumption profile of all appliances in an average Dutch household, the variables x and y are approximated from the following optimization problem as shown in Equation 3.15. This optimization problem compares the expected load profile (L) over the year to the mean of a Dutch reference profile of a household (Energie Data Services Nederland (EDSN), 2014). Multiple scenarios were considered that represent the additional electricity consumed as a function of how many people live in the house. Meanwhile, the heat produced by occupants is modeled by Equation 3.16. It is based on the human body's average heat output per person (q_{per}), scaled by the number of people in the dwelling (N_p), times a factor that considers a typical occupancy pattern. The number of people per dwelling is derived statistically from data, as given in Table 3.1.

$$min(Mismatch(x,y)) = min(\left|SLP - \overline{L(x,y)}\right|) \tag{3.15}$$

$$Q_H = q_{per} \cdot N_p \cdot \frac{L}{max(L)} \tag{3.16}$$

Table 3.1: Average number of occupants in a Dutch household in function of the typical floor areas according to EPA calculation. (Majcen et al., 2013)

Floor Area	Number of People
$A_{Floor} < 50\,\mathrm{m}^2$	1.4
$50\,\mathrm{m}^2 \leq A_{Floor} < 75\,\mathrm{m}^2$	2.2
$75\,\mathrm{m}^2 \leq A_{Floor} < 100\,\mathrm{m}^2$	2.8
$100\,\mathrm{m}^2 \leq A_{Floor} < 150\,\mathrm{m}^2$	3.0
$150\,\mathrm{m}^2 \leq A_{Floor}$	3.2

3.2.5 Advection losses

To consider advection losses inside the building, results crucial to distinguish between ventilation and infiltration losses separately. Ventilation losses, as outlined in Equation 3.17, depend primarily on the thermal properties of the air, the volume introduced into the dwelling per occupant, and the temperature difference between the ambient temperature and the interior temperature of the dwelling. Meanwhile, infiltration losses as illustrated in Equation 3.18, are similar to the ventilation losses. However, instead of the controlled volume rate per occupant, this equation considers the volume of household air that enters without proper control.

$$Q_{Ven} = \rho^{Air} \cdot C_p^{air} \cdot V_p \cdot N_p \cdot (T_{Room} - T_{Amb}) \tag{3.17}$$

$$Q_{Inf} = \rho^{Air} \cdot C_p^{air} \cdot \frac{ACH}{3600} \cdot (T_{Room} - T_{Amb}) \tag{3.18}$$

3.2.6 Heat accumulation

To account for the heat accumulation in the walls of the dwelling, the Fourier heat conduction equation 3.19 is employed, in this way, the heat conduction dynamics are taken into account. This equation establishes a connection between the surface nodes of the wall by introducing

internal nodes that consider the heat accumulation within the concrete wall. To accomplish this objective, a finite differences explicit scheme is applied, as depicted in Equation 3.20.

$$\lambda \cdot \frac{\partial^2 T}{\partial x^2} = \rho \cdot C_p \cdot \frac{\partial T}{\partial t} \tag{3.19}$$

$$T_i^{t+\Delta t} = \frac{a \cdot \Delta t}{\Delta x^2} \cdot (T_{i+1}^t + T_{i-1}^t) + (1 - \frac{2a \cdot \Delta t}{\Delta x^2}) \cdot T_i^t \tag{3.20}$$

$$a = \frac{\lambda}{\rho \cdot C_p} \tag{3.21}$$

To address heat accumulation accurately, the wall structure is simplified as depicted in Figure 3.3. In this case, heat accumulation is only considered in the concrete due to its higher mass compared to the insulation layer and the window glass. In this case, the insulation is positioned on the exterior side of the building, while the concrete wall is situated on the interior face of the building.

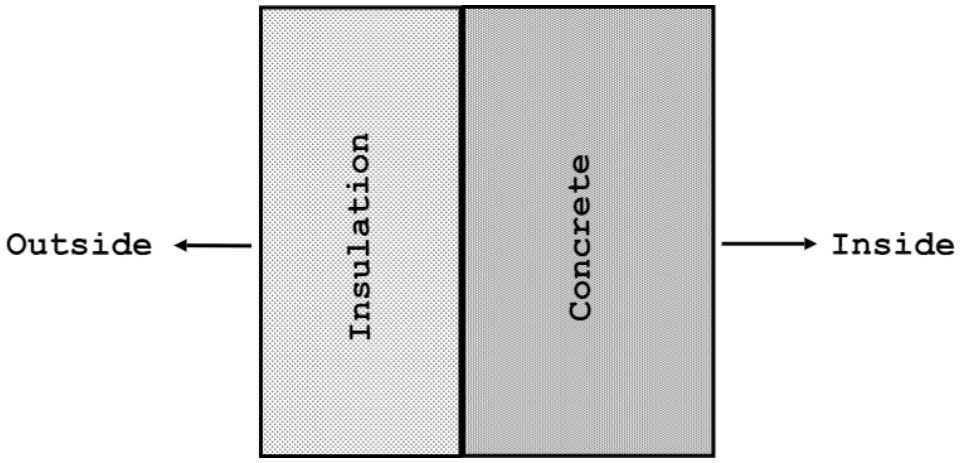

Figure 3.3: Wall structure representation that is considered in the space heating model.

3.2.7 Node balances

By taking into account all previous heat exchange modes, a node network is made considering each household. For internal surface nodes, Equation 3.22 describes the heat transfer of node i. This equation accounts for convection heat exchange between node i and the internal room air, radiation exchange with other surface walls (j), and the absorption of irradiance through the window. Also, in this way is possible to take into account the heat accumulation dynamic in the inner surface walls through conduction with internal nodes (wi) situated at the concrete wall.

$$\begin{aligned} \alpha_{conv} \cdot A_i(T_{Room}^t - T_i^t) + \alpha_{rad} \cdot \sum_{ij}^{surf.} F_{ij} \cdot A_i(T_j^t - T_i^t) + a^{Con} \cdot A_{Gl} \cdot G^{Gl} \cdot F_{wwi} = ... \\ ... - \lambda^{Con} \frac{T_{wi}^t - Ti^t}{\Delta x} + \rho^{Con} \cdot A_i \frac{\Delta x}{2\Delta t} \cdot (T_i^t - T_i^{t-\Delta t}) \end{aligned} \tag{3.22}$$

Meanwhile, a heat exchange balance over the room air is performed, where the internal air exchanges heat by convection with each internal surface and through the addition of new air volume at ambient temperature via ventilation and infiltration. Furthermore, the heat balance considers the internal heat sources (Q_{int}), including electrical consumption and human-generated heat. Additionally, the required heating (Q_{Heat}), introduced into the room by a radiator or floor

heating to maintain a reasonable temperature, is included as shown in Equation 3.23. Meanwhile, the heat exchange balance over the outside surface node, accounts for external convection, wall insulation, and heat conduction from the inside, as detailed in Equation 3.25.

$$\alpha_{conv} \sum_{ij}^{surf.} \cdot A_i(T_i^t - T_{Room}^t) + \rho^{Air} C_p^{Air}(V_p \cdot N_p + \frac{ACH}{3600})(T_{amb}^t - T_{Room}^t) + Q_{int}^t + Q_{Heat}^t = 0 \quad (3.23)$$

$$Q_{int}^t = Q_H^t + L^t \quad (3.24)$$

$$\frac{1}{1/\alpha_{conv.} + R_{ins}} \cdot A_i(T_{Amb}^t - T_{oi}^t) = \lambda_{con} \frac{T_{wi}^t - T_{oi}^t}{\Delta x} + \rho^{Con} \cdot A_i \frac{\Delta x}{\Delta t} \cdot (T_{oi}^t - T_{oi}^{t-\Delta t}) \quad (3.25)$$

Heat exchange balances over the nodes are considered through Equations 3.22, 3.23, and 3.25. By considering all this equations, it results possible to solve the system of equations and calculate temperatures in each node for every hour of the year, including the inside temperature of every house/apartment. With this input of inside temperatures of households, one can find out what the necessary amount of heating needs to be injected into the household.

3.2.8 Model design

Either, the room temperatures or the heating/cooling profiles of each dwelling, can be used as inputs for the proposed set of equations. In the case of this project, the temperature that turns off the heating system, which usually is between $18°C$ and $24°C$, and the temperature where cooling is turned on, are used as inputs in the selected methodology. In this way, the temperature evolution of all nodes and their heating/cooling demand is computed. Figures 3.4b, 3.5a, and 3.5b present the estimated temperature evolution and the required heating/cooling production to reach that temperature for each node for the house in Figure 3.4a.

Additionally, as illustrated in Figure 3.5a and Figure 3.5b, both heating and cooling demands change drastically each hour. Which in reality, is not possible due to the thermal inertia inherent in supply heating systems. This led to the adoption of a strategy involving the averaging of daily heating and cooling demands, illustrated in Figure 3.6a and Figure 3.6b, respectively. In this way, by using the daily average heating and cooling, the node's set of equations is solved by using those profiles as an input, which produces the temperature evolution in Figure 3.7.

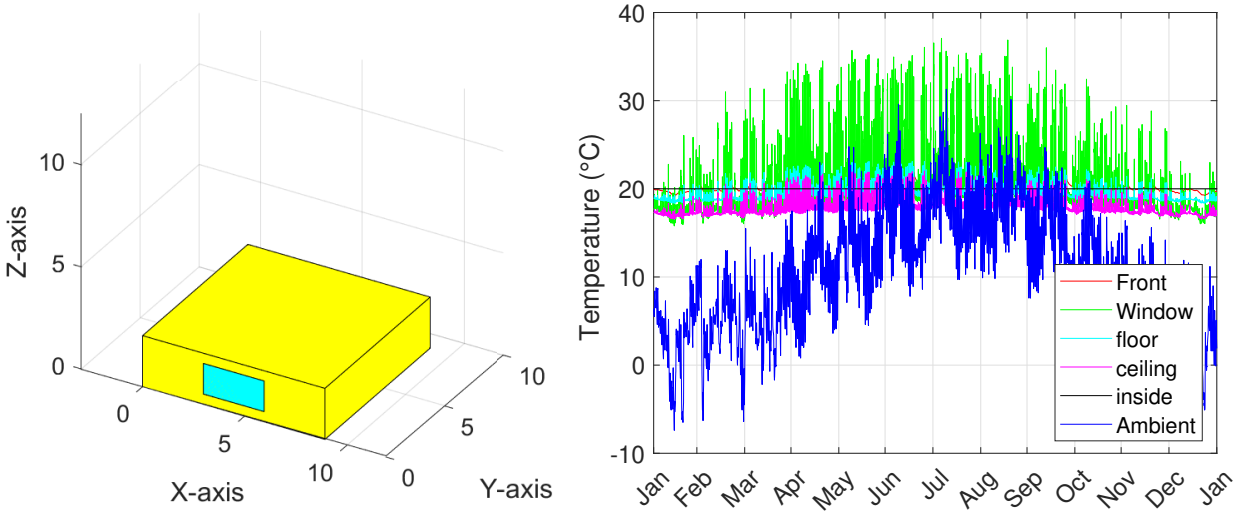

(a) House to be modeled

(b) First set of yearly temperatures

Figure 3.4: Representation of the modeled building and the inside temperatures during the whole year. (a) Example of modeled building. (b) Temperature profile of the modeled house in (a). [For a house in Delft with a floor area of 80 m^2, a ceiling height of 2.5 m, and a high insulation level.]

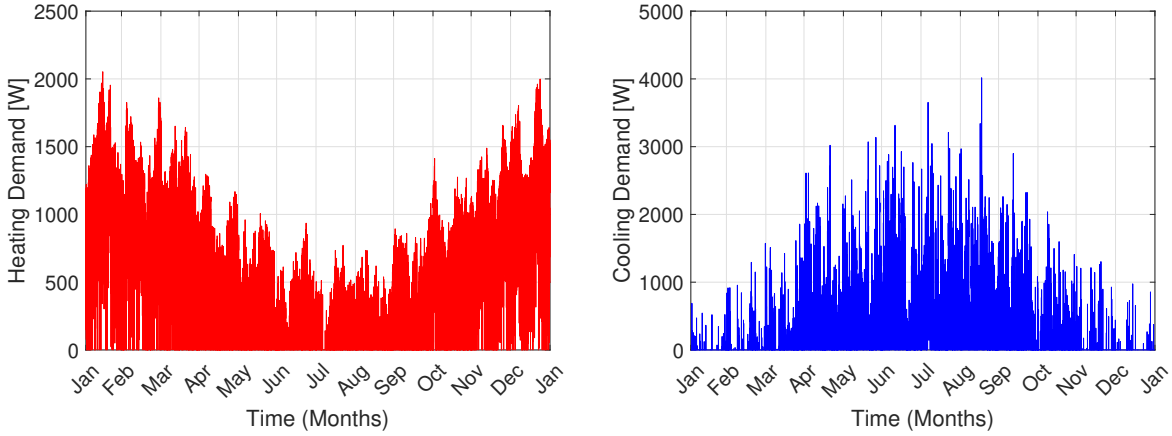

(a) Heating demand

(b) Cooling demand

Figure 3.5: First approximations of the heating and cooling demand for the modeled house in Figure 3.4a. [For a house in Delft with a floor area of 80 m^2, a ceiling height of 2.5 m and a high insulation level.]

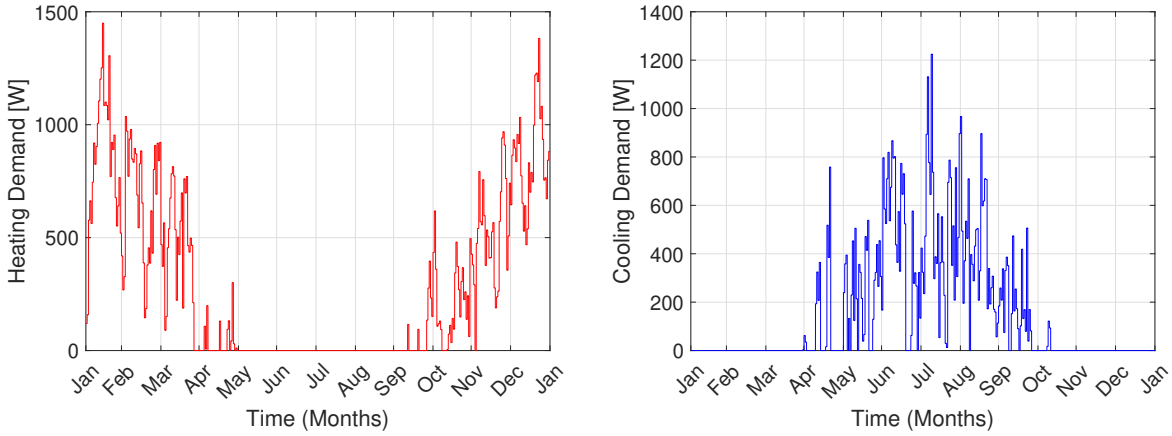

(a) Heating demand

(b) Cooling demand

Figure 3.6: Final heating and cooling demand for the modeled house in Figure 3.4a, by using the average daily heating and cooling demand. [For a house in Delft with a floor area of 80 m^2, a ceiling height of 2.5 m and a high insulation level.]

As observed in Figure 3.7, a constant room temperature is not achieved as observed in the "Inside Temperature" (black line). However, the average room temperature remains consistent with the temperature range, fluctuating between $18°C$ and $25°C$. This inside room temperature fluctuation is significant during the day, which changes daily mainly due to the changing weather conditions and internal heat production.

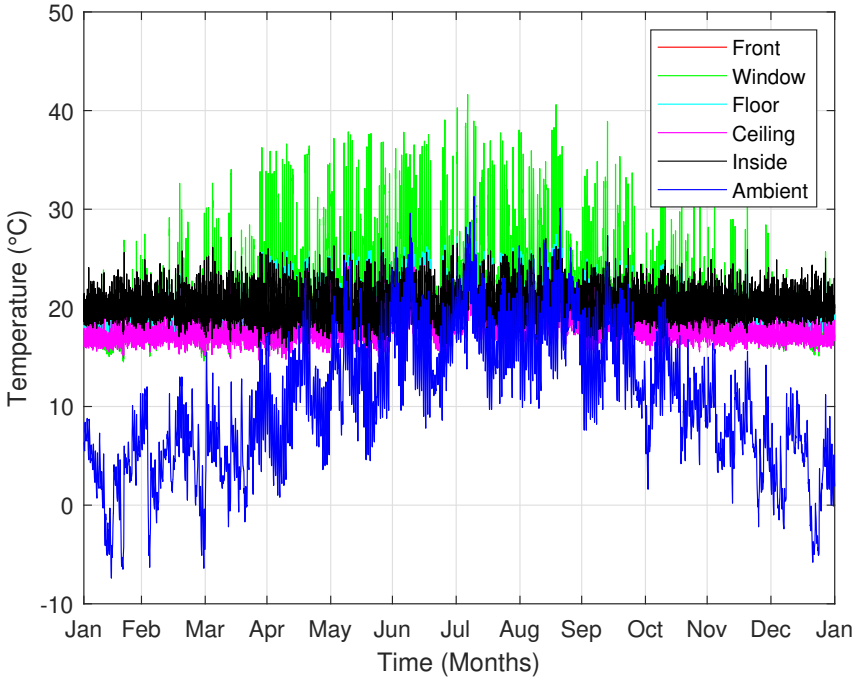

Figure 3.7: Final temperature profile for the modeled house in Figure 3.4a, by using the average daily heating and cooling demand. [For a house in Delft with a floor area of 80 m^2, a ceiling height of 2.5 m and a high insulation level.]

3.3 Domestic hot water demand model

For the domestic hot water model, a simplified methodology to the one used for electrical consumption is applied, as outlined in Equation 3.26 and Figure 3.27. Using data from Ahmed et al. (Ahmad et al., 2020), it is possible to construct a heat demand model that provides daily load profiles converging with the standard load profile. This is achieved through Equation 3.27 and by obtaining the probabilities of DHW consumption within a household. Figure 3.8 illustrates the average DHW demand over the entire year obtained from the DHW model.

$$DHW = \sum_{i=1}^{\#flows.} \dot{m}_{DHW} \cdot g_{DHW}(P_{Sea}(x,t), P_H(y_i)) \tag{3.26}$$

$$min(Mismatch(x,y)) = min(\left|SLP_{DHW} - \overline{DHW(x,y)}\right|) \tag{3.27}$$

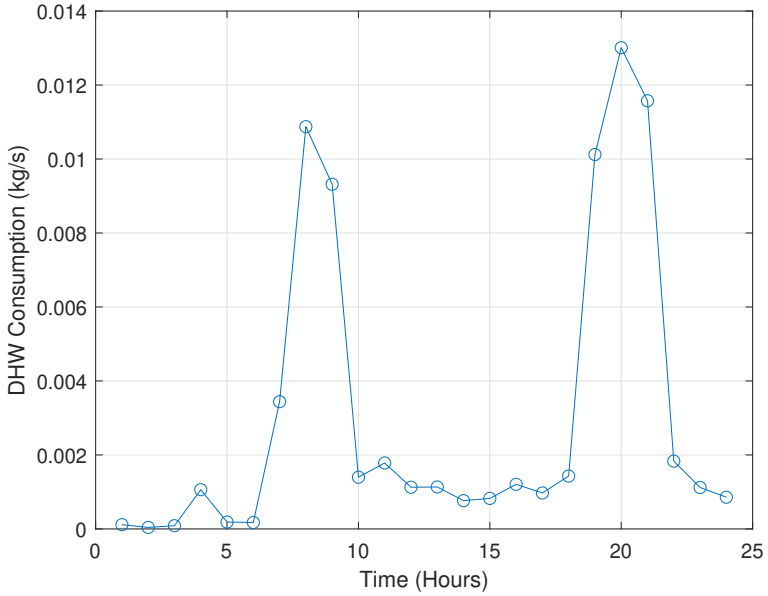

Figure 3.8: Average daily domestic hot water profile for a standard occupant in The Netherlands through the DHW model. [For a house with a floor area of 80 m^2, a ceiling height of 2.5 m and a high insulation level.]

3.4 Validation

The validation of the heat demand model consist in reproducing and testing the cases defined by Nieboer et al. (Nieboer & Filippidou, 2014). In this way, results possible to determine to what extent there is a deviation of the space heating model concerning the data from Nieboer et al. The different dwellings considered are classified in Table 3.2 below, which embodies the key characteristics of the data taken from Nieboer et al. It is also assumed that there is a dwelling height of 2.5m, and the geometry is square for each dwelling for comparison purposes. An average internal heat production is considered by assuming an average occupant within the model.

Table 3.2: Main building characteristics of the analyzed house types. (Nieboer & Filippidou, 2014)

Type of House	No. of Dwellings	No. of Stories	No. of Neighbors	Usable Floor (m^2)
Detached House	1	2	0	170
Semi-Detached House	1	2	1	148
Terraced (Mid-Row)	1	2	2	124
Terraced (End-Row)	1	2	2	124
Multifamily Building	27	4	0	2756
Gallery Flat	26	4	0	2941

In this validation process, two insulation levels are examined in several building types. These insulation levels are summarized in Table 3.3. The initial case consist of the Actual Dutch Regulation mandated for new buildings in the Netherlands (ADR). In contrast, the second case consists of better thermal properties that could be implemented to make buildings achieve the label Net Zero Energy Building (NZEB).

Table 3.3: Buildings thermal insulation data. (Nieboer & Filippidou, 2014)

Case	R_{fa} Façade (m^2K/W)	R_r Roof (m^2K/W)	U Windows ($W/m^2/K$)
Minimum Insulation	3.5	4	1.65
NZEB Proposal	5	5	1

By using the heat space heating model throughout the entire year, the estimation accurately predicts each scenario in the NZEB case with a relative average deviation of 1.8%. Still, when there is lower-quality insulation as the minimum insulation requirement, the model approximates with less accuracy the required heating with a relative average deviation of 6.6%. This variance can be attributed to the less precise estimation of the building's geometry. This situation contrasts with the NZEB, where the robust insulation significantly reduces the impact of assumptions, as depicted in Table 3.4.

Table 3.4: Required annual heating demand per dwelling area.

Type of House	Minimum Insulation Requirement		NZEB Proposal	
	Data (kWh/m^2)	Model (kWh/m^2)	Data (kWh/m^2)	Model (kWh/m^2)
Detached House	72	68	41	41
Semi-Detached House	66	63	37	38
Terraced (Mid-Row)	61	57	33	32
Terraced (End-Row)	66	60	33	35
Multifamily Building	57	57	28	33
Gallery Flat	59	51	30	28

3.5 System integration

3.5.1 PVT model and solar collector

The two key variables of the solar collector models are the outlet temperature of the working fluid and the mass flow rate of the working fluid. By considering both variables, it is possible to determine the energy state of the fluid which makes possible a proper integration with every

other model, while ensuring that the temperature requirements of SH technology and DHW are met. The reduced temperature approach is applied when predicting the heat generated by the PVT or ST module for the thermal performance prediction of a solar collector.

The performance of the system is a function of the working fluid inlet temperature. In the case, that the inlet temperature is nearly close to the ambient temperature, the thermal efficiency is high. This means that in a string of several modules, the first ones within the string will perform with high thermal efficiency, while the last ones will exhibit a lower thermal efficiency because the inlet temperature of those modules will be higher. For the scope of this project, two types of modules are considered, an unglazed flat plate PVT module and a glazed flat plate ST module as indicated in Figure 3.9.

$$Q^{PVT} = \dot{m}^{PVT} C_p^{Water} (T_{out}^{PVT} - T_{in}^{PVT}) \tag{3.28}$$

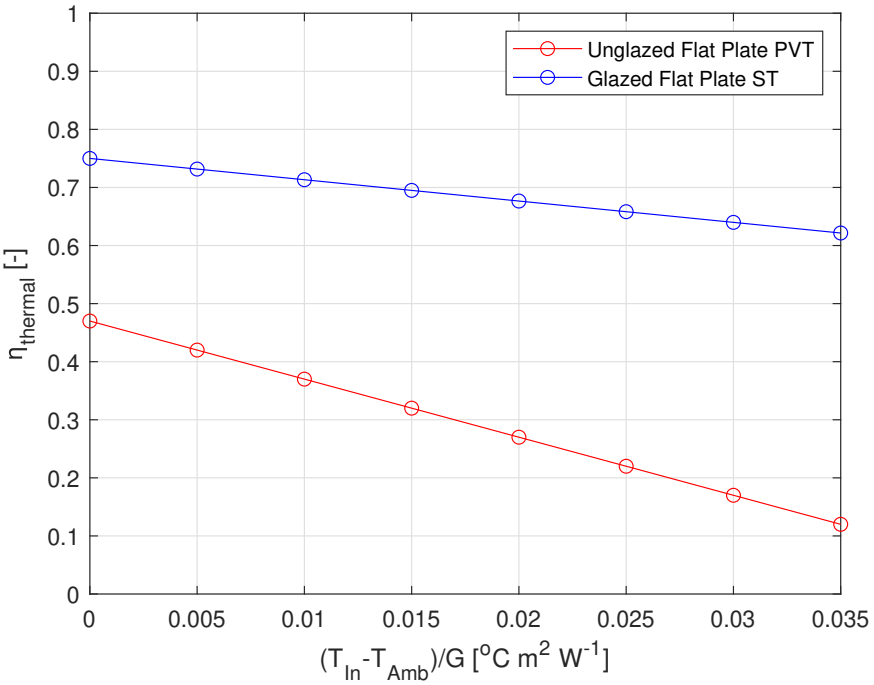

Figure 3.9: Thermal efficiency of the used PVT and ST module in function of the reduced temperature. [An unglazed flat plate PVT and a glazed flat plate ST module are considered in the integration of the system. Both modules are water-based with an area of $2.0m^2$ per module.]

3.6 Operational modes

The operational modes are described in more detail for a detached house with an area of 80 m^2 in Delft, maintaining an average inside temperature of $20°C$ and using only one PVT module. This setup allows for a detailed demonstration of the overall dynamics of each operational mode and the heat produced and supplied for space heating demand in this scenario.

3.6.1 Mode 1 - Summer mode

Solar collector to heat demand

This operational mode operates when the solar collector raises the temperature of the working fluid flow, as outlined in Equation 3.29 and 3.30, to supply heat to the SH or DHW system,

respectively. Therefore, this operational mode considers the mass flow rate and its temperature during each hour of the year to provide heat whenever is needed. Consequently, the amount of heat provided by this mode throughout the year is relatively low, as depicted in Figure 3.10a. This is primarily because the highest temperatures are typically reached during the summer months, as illustrated in Equation 3.28. As a result, a significant portion of the generated heat remains unused due to no heating demand in the summer.

$$T_{out}^{PVT} > 30 - 0.5T_{Amb} \tag{3.29}$$

$$T_{out}^{PVT} > 60°C \tag{3.30}$$

Excess heat to ATES

During the whole year a large part of the produced heat from the solar collector occurs during the summer period, which mostly goes unused since, in this period, there is no need for heating in the households. The working fluid, in this case, is pumped into the hot aquifer of the ATES system for storage. Figure 3.10a illustrates the heat produced by one PVT module together with the heat demand for a house in Delft with a floor area of 80 m^2, a ceiling height of 2.5 m and a NZEB insulation, which would be lost if it is not stored for seasonal storage. In contrast, Figure 3.10b provides the amount of space heating delivered from this summer mode, considering system efficiencies and the lack of match between heat production and consumption.

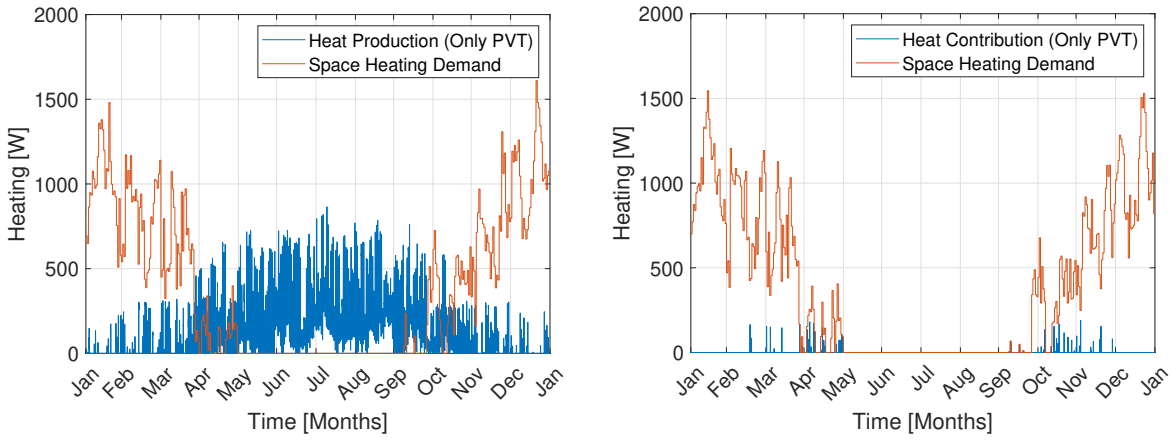

(a) Heat demand and PVT heat production using a single PVT module of 2 m^2.

(b) Heat demand and heat supplied in summer mode using a single PVT module of 2 m^2.

Figure 3.10: Space heating demand in a detached house from which heat is supplied using summer mode. (a) Space heating demand and total heat produced by a PVT module. (b) Space heating supply and total heat supplied to the house using summer mode. [For a house in Delft with a floor area of 80 m^2, a ceiling height of 2.5 m, an NZEB insulation, and a single PVT module of 2 m^2.]

3.6.2 Mode 2 - Spring mode

This second operational mode operates when the condition described in Equation 3.29 is not met, or when the heat provided by the "Summer mode" is insufficient. By utilizing the heat pump, a higher temperature can be achieved, enabling the system to partially fulfill the heating demand for space heating and domestic hot water. For the case of space heating, this operational mode is expected to operate during the entire year, except for summer when there is no expected heating demand, as illustrated in Figure 3.11a. Meanwhile, Figure 3.11b indicates the expected daily average heat pump COP which is considerably constant while the heat pump is running.

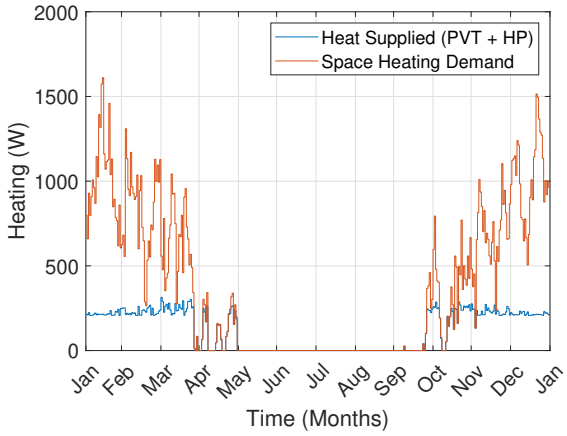

(a) Heat demand and PVT-HP heat production using a single PVT module of 2 m^2.

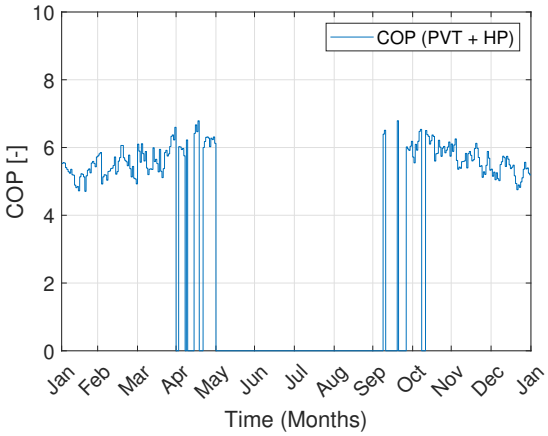

(b) Operational Heat Pump COP.

Figure 3.11: Space heating demand in a detached house from which heat is supplied using operational mode 2. (a) Space heating demand and total heat produced by a PVT-HP coupling. (b) HP COP coefficient during the whole year. [For a house in Delft with a floor area of 80 m^2, a ceiling height of 2.5 m, an NZEB insulation, and a single PVT module of 2 m^2.]

3.6.3 Mode 3 - Winter mode

This operational mode is employed when the other operational modes are unable to fulfill the entire heat demand of the household. Figure 3.12b shows the heat contributions of Summer Mode and Spring Mode while using a single PVT module of 2 m^2, indicating that it is not possible to meet the entire demand in winter. Therefore, it is necessary to use Winter Mode, as illustrated in Figure 3.12a, to fulfill the heat demand. The overall contribution of this mode is crucial for sizing the solar collector system. This is because the heat provided by this mode should be produced by Summer Mode during summer and stored for winter, ensuring a net zero balance.

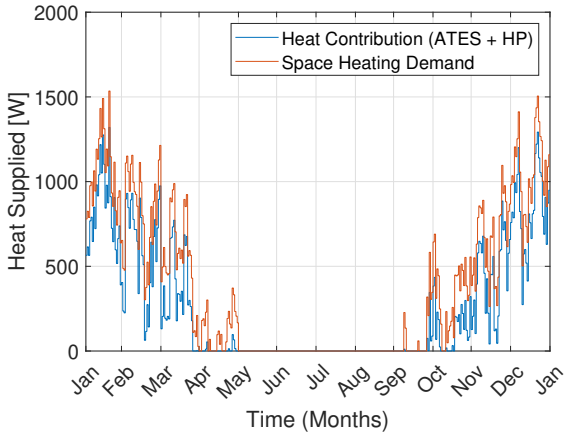

(a) Supplied heat through winter mode (ATES + HP) while using a single PVT module of 2 m^2..

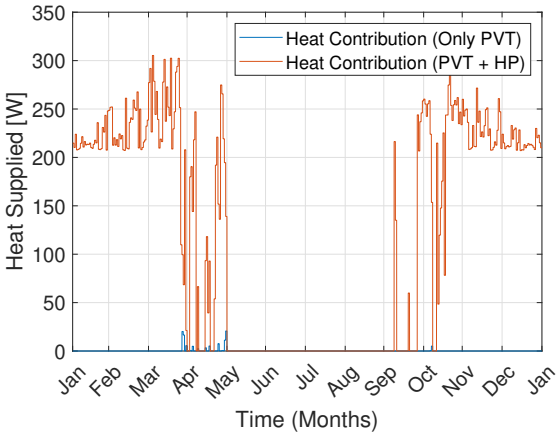

(b) Heat supplied by mode 1 and mode 2 while using a single PVT module of 2 m^2.

Figure 3.12: Space heating demand in a detached house from which heat is supplied using operational mode 3. (a) Space heating demand and total heat produced by the ATES-HP coupling. (b) Supplied heat by using directly a PVT module (mode 1) and the PVT-HP coupling (mode 2). [For a house in Delft with a floor area of 80 m^2, a ceiling height of 2.5 m, and a high insulation level.]

3.7 Conclusions

The developed space heating model simulates thermal demand in individual dwellings or clusters, offering a simplified yet effective approach. This model requires only basic building characteristics, making it user-friendly. Integrated into the PVMD Toolbox, it allows users to adjust thermal properties to simulate various household types, from poorly insulated to highly insulated dwellings. By validating this model based on a thermal resistance network, the model accurately estimates heat demand based on building geometry and thermal properties.

By integrating this heat demand model with other system components, several operational modes were structured to approximate the options for meeting this heat demand. These operational modes cover how heat exchange is managed throughout the year, fulfilling each component's thermal and energy requirements, including the necessary temperatures for each thermal application.

The main conditions for these operational modes depend on the outlet temperature of the solar collector system and the heat demand. For the Summer mode, it activates when the outlet temperature of the solar collector system exceeds the minimum required by the heating supply system. If there is still an unmet heating demand, the Spring mode begins, utilizing residual heat from the Summer mode (or directly from the solar collector system if summer mode was not used) to supply heat to households. If additional heating is still needed, the Winter mode is activated, drawing heat from the ATES system.

Chapter 4

Heat Demand Sensitivity and Influence over System Sizing

A sensitivity analysis is conducted across the integrated system to evaluate its overall behavior. This involves examining various parameters to understand the impact of building thermal characteristics, design, solar module configuration, and occupant behavior. Specifically, two distinct scenarios are explored for building thermal insulation: one following Dutch regulations and the other meeting NZEB standards.

Additionally, two building typologies are considered: detached buildings and mid-row terraced houses, as depicted in Figures 4.1a and Figure 4.1b, respectively. Subsequently, the configuration of PVT, PV and/or ST modules are explored, focusing on the arrangement of modules in series or parallel and their implications for the final output. Finally, the analysis considers the desired internal temperature dynamics of a building, as an approach to approximate occupant behavior.

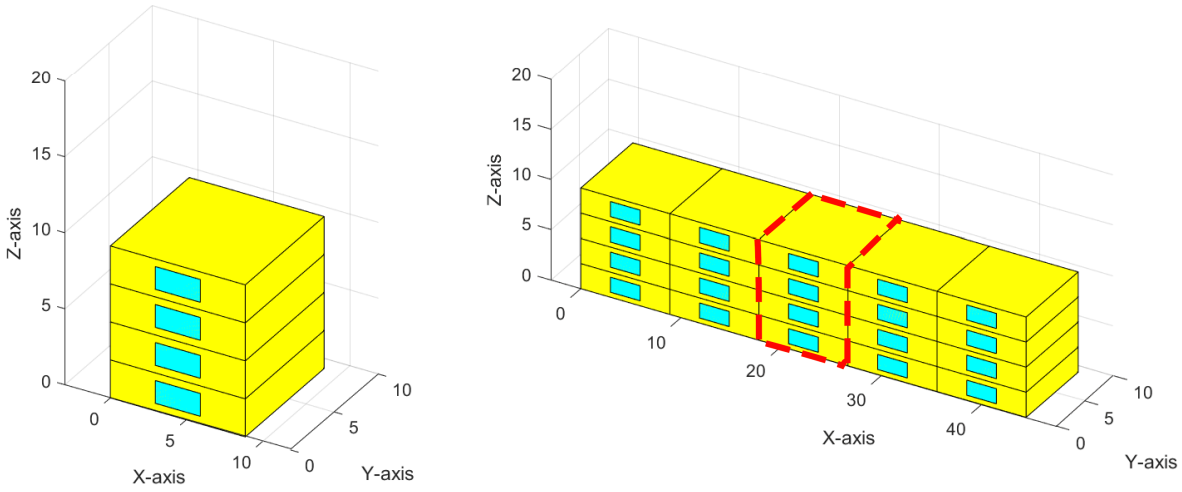

(a) Representation of a detached house.

(b) Representation of a mid-row building.

Figure 4.1: Detached and mid-row buildings representation as buildings that can be modeled using the space heating model.

4.1 Space heat demand sensitivity

To assess the importance of building characteristics in heat demand, and hence system size, two scenarios are distinguished about the impact of building characteristics: the Dutch regulation

scenario and the NZEB scenario, as set out in Table 3.3. In such cases, the effect of introducing higher quality insulation to the building will be reflected in the demanded heat for each apartment and, consequently, in the system sizing required to cope with that demand. The ADR case deals with the same thermal classification used in the validation (see Section 3.4).

4.1.1 Building characteristics and thermal insulation

To analyze the sensitivity of the system, the space heating demand of a mid-row building is studied as a function of the number of stories, as shown in Figure 4.2a. In both cases, whether the mid-row building has NZEB insulation or ADR insulation, the annual space heating demand per unit area tends to stabilize as the number of stories increases. The difference between the two insulation cases lies in the total amount of heat needed per area, but the overall behavior remains identical.

This stabilization in both thermal insulation cases occurs because, with more stories, the middle apartments are less influenced by the top apartment, which has higher heat requirements due to increased heat losses from its greater surface area exposed to the environment. Consequently, this saturation at a stable value is expected. In contrast, Figure 4.2b illustrates how the annual space heating profile varies with the number of stories.

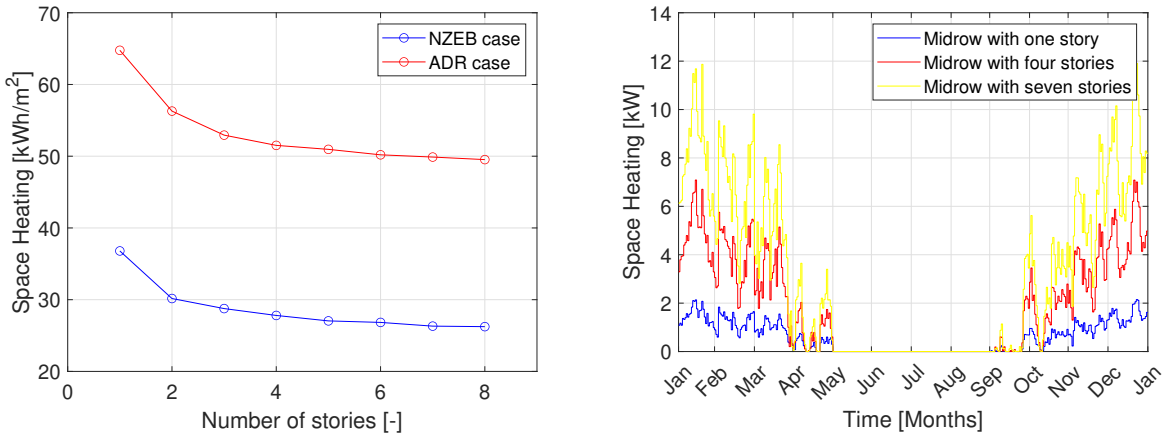

(a) Total space heating consumption of a residential mid-row building in function of the total amount of stories.

(b) Space heating profiles of a residential mid-row building with NZEB insulation.

Figure 4.2: Annual Space Heating Consumption and Profile Demand for Residential Buildings: Comparison of Insulation Cases and Story Levels. (a) Annual space heating consumption per floor space of whole residential buildings in function of the total number of stories considering two insulation cases: Net zero energy building case (NZEB) and Actual Dutch Regulation Case (ADR). (b) Space heating profile demand of three residential mid-row buildings with different number of stories. [For a midrow building with a floor area of 80 m^2 per dwelling in the city of Delft, an average inside temperature of 20°C was considered.]

Floor area

By considering the influence of floor area over a four-story mid-row building and a four-story detached building, as shown in Figure 4.3, the total heating demand throughout the year exhibits a linear relationship with respect to the apartment floor area. This linear trend is observed in both types of buildings; however, the detached building has higher thermal demands due to a larger surface area in contact with the environment, leading to more heat losses.

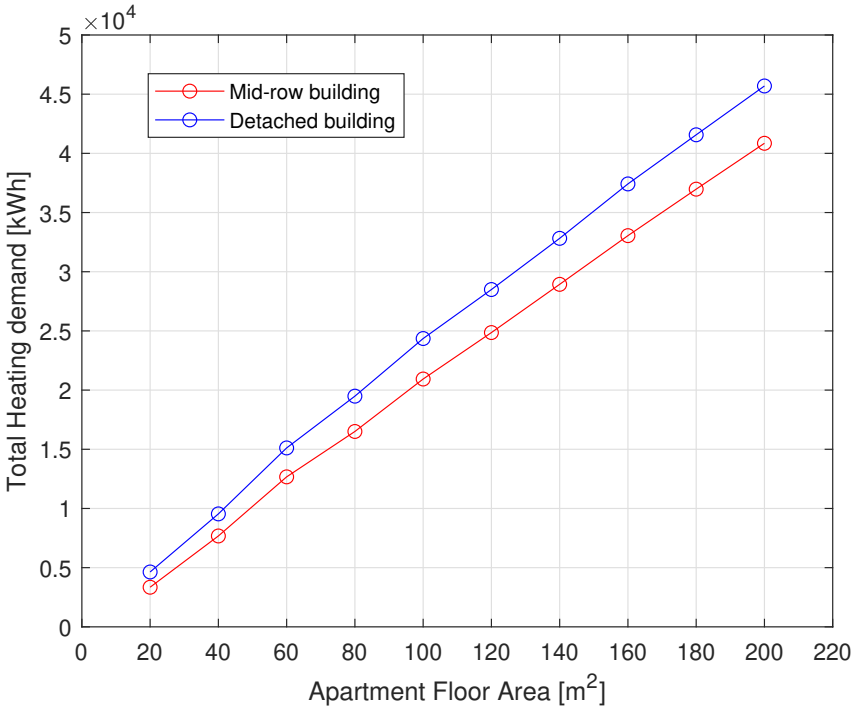

Figure 4.3: Annual space heating demand in function of the apartment floor area. [For a four-story building in the city of Delft, considering an average inside temperature of 20°C.]

4.1.2 Inside temperature influence

To estimate the influence of occupant behavior over the overall space heating demand, the desired indoor temperature is used as a key parameter. By varying this parameter in a mid-row four stories building, it is possible to illustrate the impact of high-energy consumers, which are represented by a desired temperature of 24°C, compared to low-energy consumers with a desired temperature of 18°C.

This influence is depicted in Figure 4.4a, which shows that heating consumption exhibits a non-linear behavior with both insulation cases. However, when considering an inside temperature range between $18°C$ and $24°C$, the behavior is almost linear. Additionally, by comparing the annual heat demand of low-energy consumers with high-energy consumers, it is notable that the annual heating requirement for high-energy consumers is approximately twice as high. The overall heat demand behaves similarly between both cases as shown in Figure 4.4b, but the six degrees difference increases the overall heat demand to almost double.

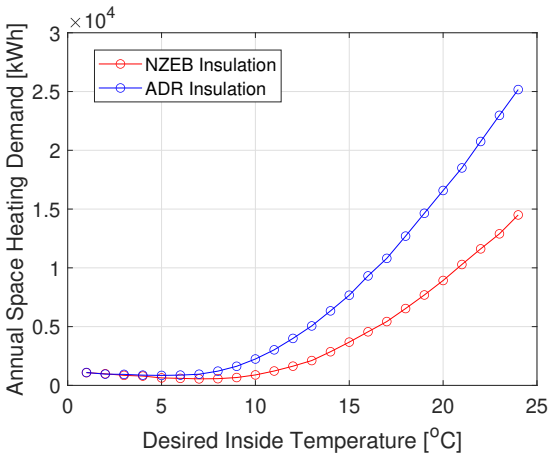

(a) Annual SH demand for two thermal insulations, NZEB case and ADR case.

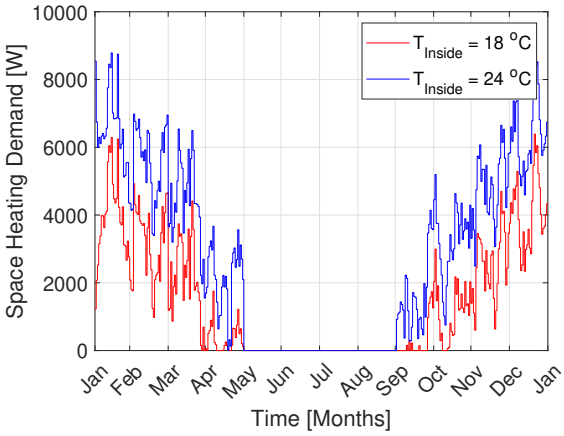

(b) SH demand over the year by setting two different inside temperatures.

Figure 4.4: Annual Space heating demand based on inside desired temperature and insulation types. (a) Annual space heating demand in function of the inside desired temperature with two types of insulation, NZEB insulation and ADR insulation. (b) Space heating demand over the whole year by setting the inside temperature at two conditions by while considering the ADR case. [For a mid-row building with four stories with a floor area of 80 m^2 per dwelling in the City of Delft was considered.]

4.2 System sensitivity and sizing

The sensitivity analysis of the main building characteristics will be used not only to quantify the change in the heat demand profiles but also the final solar collector system sizing and configuration. In this way, it results possible to determine the dependence of the system sizing over the basic building design.

4.2.1 Type of collector

In the case of PVT and ST modules, it is essential that modules in the exact string are identical since they share a standard mass flow. The primary sizing on the side of the solar collector involves the determination of the number of modules per string and the number of strings that are going to be required to supply the heat demand. Hence, the water flow output from one module in a string becomes the inlet for the next module. Figure 4.5 depicts a schematic of a possible number of modules per string. In this way, the same mass flow is maintained even when more modules are added per string. This has the same thermal effect as using a single module and dividing the mass flow accordingly by the number of modules per string.

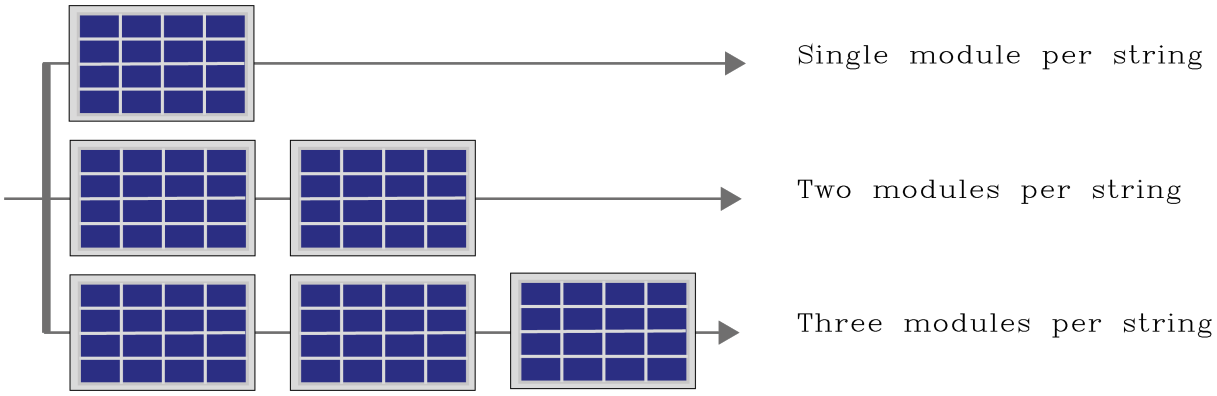

Figure 4.5: Representation of the possible solar collector configuration per string, while considering the same amount of mass flow passing through the PVT string.

To properly understand the thermal behavior of adding more PVT modules per string, Figure 4.6a illustrates the daily average outlet temperature when using two PVT modules per string compared to a single PVT module per string. Figure 4.6a clearly shows that during the winter months, there is almost no considerable improvement in adding more modules per string, while in the summer months, the improvement in the final flow temperature is considerable. This remarks the importance of seasonal heat storage, using surplus heat from summer months to meet winter demand. However, it is important to note that adding a large number of modules per string will not result in a permanent temperature improvement. As shown in Figure 4.6b, increasing the number of PVT modules per string will raise the temperature only to a certain maximum point. In this situation, the working fluid can no longer effectively extract heat from the PVT modules.

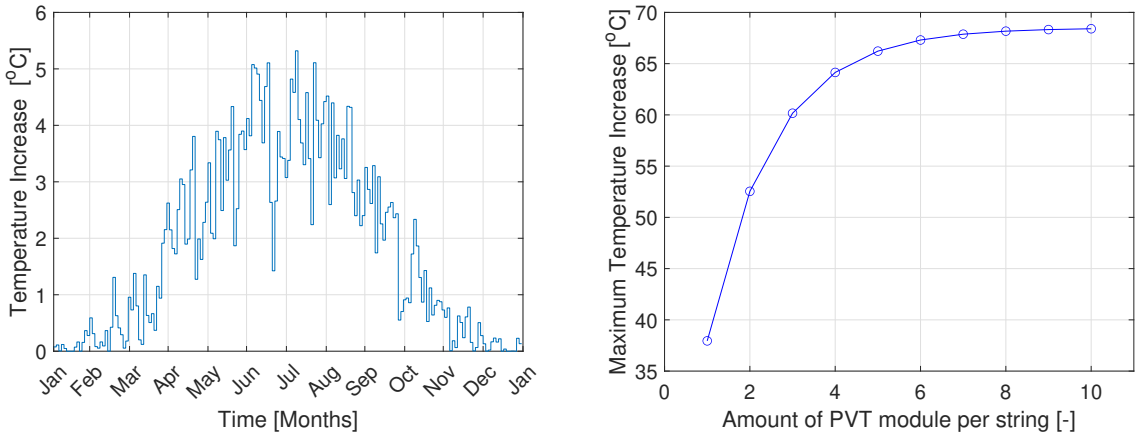

(a) Temperature difference between two PVT modules per string and a single PVT module per string.

(b) Maximum fluid temperature during the whole year by using several PVT modules per string.

Figure 4.6: Temperature change by increasing the number of modules per string. (a) Temperature difference between two PVT modules per string and a single PVT module per string. (b) Maximum fluid temperature during the whole year by using several PVT modules per string. [Estimated at the City of Delft with water-based PVT modules of 2.0 m^2 with no tilt angle.]

On the other hand, a comparison between the temperatures obtained from a PVT module and an ST module is shown in Figure 4.7a. It is evident that the temperature output from the ST module is considerably higher than the outlet temperature obtained throughout the PVT module during the whole year. This indicates that the ST module performs better than the PVT module in terms of heat production. More specifically, the ST module consistently achieves higher temperature increases than the PVT module whenever there is any irradiation during the day, as illustrated in the first week of the year in Figure 4.7b.

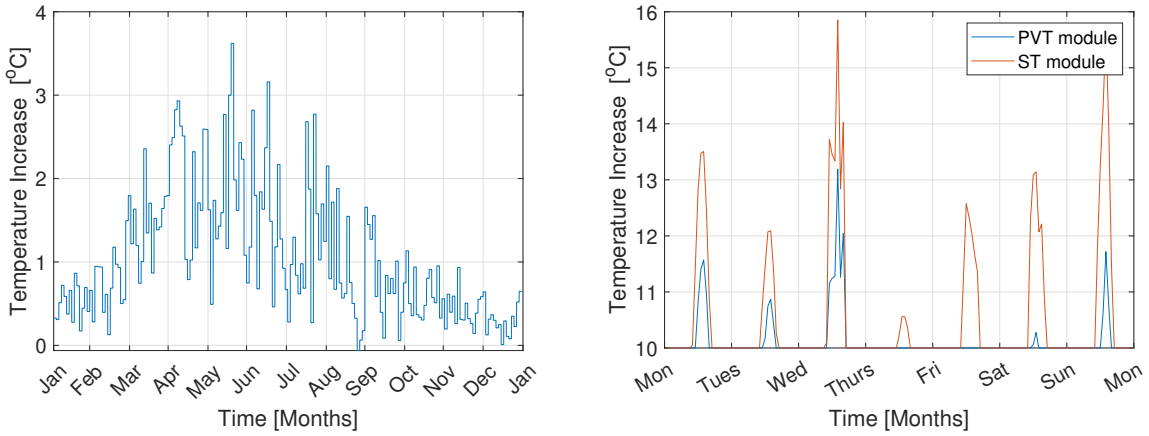

(a) Output comparison between the water output temperature between the ST module respect to the PVT module.

(b) Outlet water temperature coming from the PVT module and the ST module, during the first week of the year.

Figure 4.7: Temperature difference while comparing the thermal behavior of the PVT module and the ST module. (a) Output comparison between the water output temperature between the ST module respect to the PVT module. (b) Outlet water temperature coming from the PVT module and the ST module, during the first week of the year. [Estimated in the City of Delft was considered with water-based PVT modules of 2.0 m^2 with no tilt angle.]

4.2.2 Solar collector sizing and configuration

Building stories

By considering the influence of building stories on space heating demand, it is possible to analyze necessary amount of modules to meet this demand, as shown in Figure 4.2a and Figure 4.2b for the NZEB and ADR cases, respectively. In these scenarios, two configurations are examined: the ST/PV configuration and the PVT/PV configuration. The ST module and the PVT module supply heat to meet the space heating demand as described in Summer mode and Spring mode, with any excess heat being supplied to the ATES system throughout the year. This approach achieves a net thermal balance by fulfilling the household's thermal requirements while providing an equal amount of heat to the ATES system as the one extracted from it.

The term "net electrical balance" refers to the scenario where the electrical production from the PVT module and/or PV module meets the entire electrical consumption of the heat pump in any configuration. Meanwhile, "net thermal balance" denotes the fulfillment of either the space heating demand and the domestic hot water demand. Although an ST/PVT configuration can be analyzed, it is generally less favorable as it requires more modules than other configurations. Consequently, the ST/PVT configuration is not ideal when the ATES system can easily supply the necessary heat demand.

Both Figure 4.8a and Figure 4.8b indicate that only using PVT modules achieves a better area optimization compared to using ST and PV modules for reaching net thermal and net electrical requirements for the whole building. More remarkably, it is notable that by increasing the number of stories per building, which is represented by an almost linear increase over the total space heating as shown in the stabilization in Figure 4.2a, the necessary solar collector area increases similarly in a linear behavior.

Additionally, it is shown that increasing the number of modules per string leads to an increase in the total area needed to fulfill thermal and electrical demands. However, it is also evident that the energy utilization of the area improves with the number of strings. Specifically, when

using two modules per string, the required area increases, but it is less than double the initial area. Nevertheless, only using a single module per string requires less roof area usage.

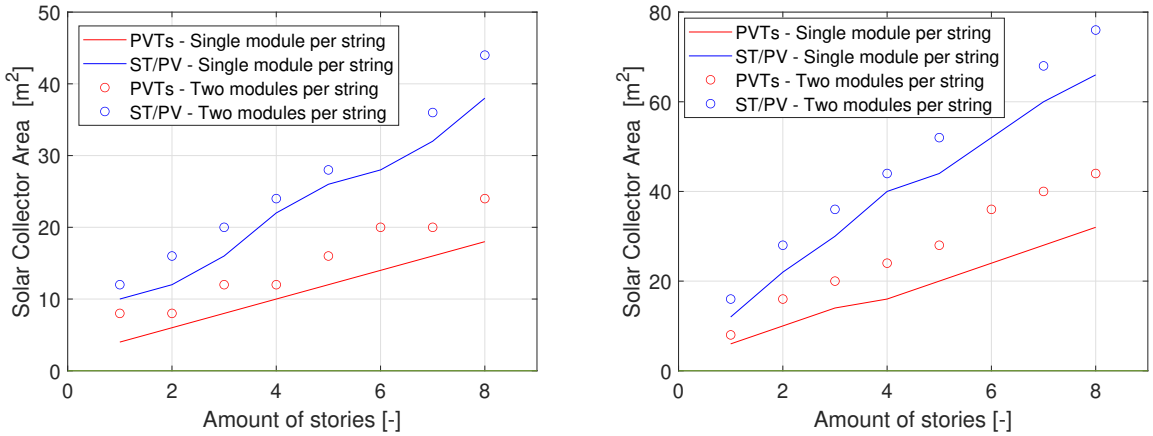

(a) Mid-row four stories building with NZEB insulation. (b) Mid-row four stories building with ADR insulation.

Figure 4.8: Required solar collector area over two types of configurations to achieve net thermal production and net electrical consumption over a four stories mid-row building. In which two insulation cases are used: (a) NZEB insulation case and (b) ADR case. [Considering a floor area of 80 m^2 per dwelling in the City of Delft with an average inside temperature of 20°, together with water-based PVT modules of 2.0 m^2 with no tilt angle.]

Apartment floor area

Given the clearly linear behavior of the total heating demand in Figure 4.3 with respect to the apartment floor area of a mid-row four-story building, the required number of modules for various configurations is estimated and shown in Figure 4.9. Similarly, a linear relationship is observed concerning the total number of modules needed to achieve net exchange in thermal and electrical energy throughout the year.

When comparing all three configurations, the only PVT and PVT/PV configurations require similar amounts of roof area. In contrast, the ST/PV configuration needs significantly more area to achieve net energy conditions. However, in all cases, the required solar collector area is far less than the available roof area, indicating that it is technically feasible to use any of the three configurations.

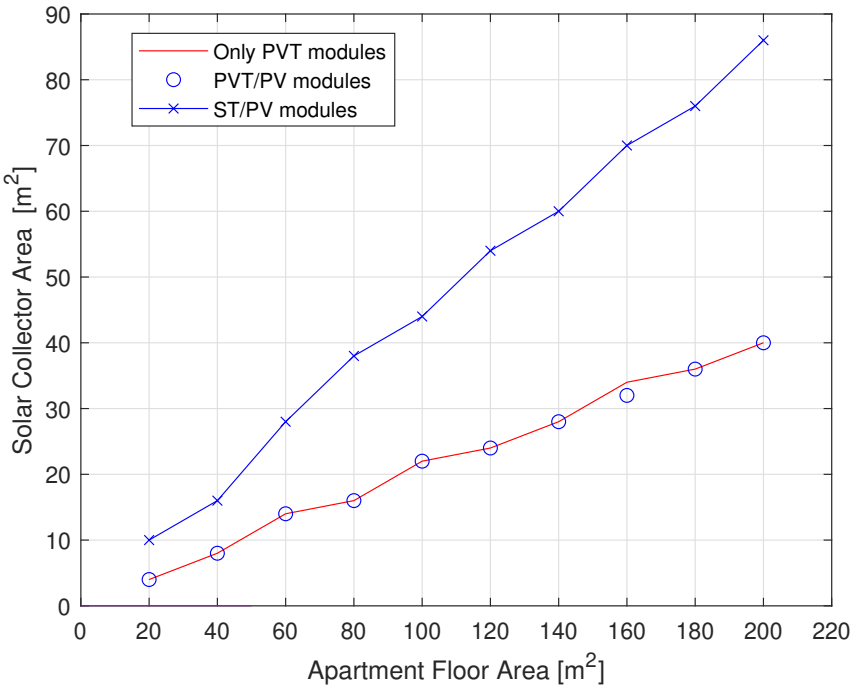

Figure 4.9: Required solar collector area to achieve net thermal production and net electrical consumption over a four stories mid-row building by considering several apartment floor areas. [Considering a floor area of 80 m^2 per dwelling in the City of Delft with an average inside temperature of 20°, together with water-based PVT modules of 2.0 m^2 with no tilt angle. STs/PVs Type: ST modules for heating and PV modules for electricity. PVTs/PVs Type: PVT modules for heating together with a contribution to the electrical demand that is fulfilled by PV modules. All calculations use a single solar collector per string.]

Desired temperature

As commented previously, the desired temperature in each household significantly impacts the overall heat demand, as illustrated for the case of a mid-row four-story building in Figure 4.4a. By analyzing the inside temperature between $18°C$ and $24°C$, it is possible to estimate the required solar collector area needed to achieve net energy exchange conditions. These estimates, shown in Figure 4.10, compare two scenarios: using only PVT modules and using an ST/PV configuration with one module per string. The configuration of only PVT modules requires around half the solar collector area to achieve net energy exchange conditions for every analysed temperature.

As illustrated, it is clear that the difference in the required solar collector area for maintaining a desired temperature inside the building between $18°C$ and $24°C$ is significant, in both cases. Nearly double the area is required to maintain a temperature of $24°C$ compared to $18°C$. However, in all cases, the required solar collector area is less than the available roof area. This indicates that if the type of occupant is unknown, which is probably the case in new residential buildings, it is possible to install additional PVT modules on the roof to produce enough heat and electricity for the building, in the case of undersizing the system.

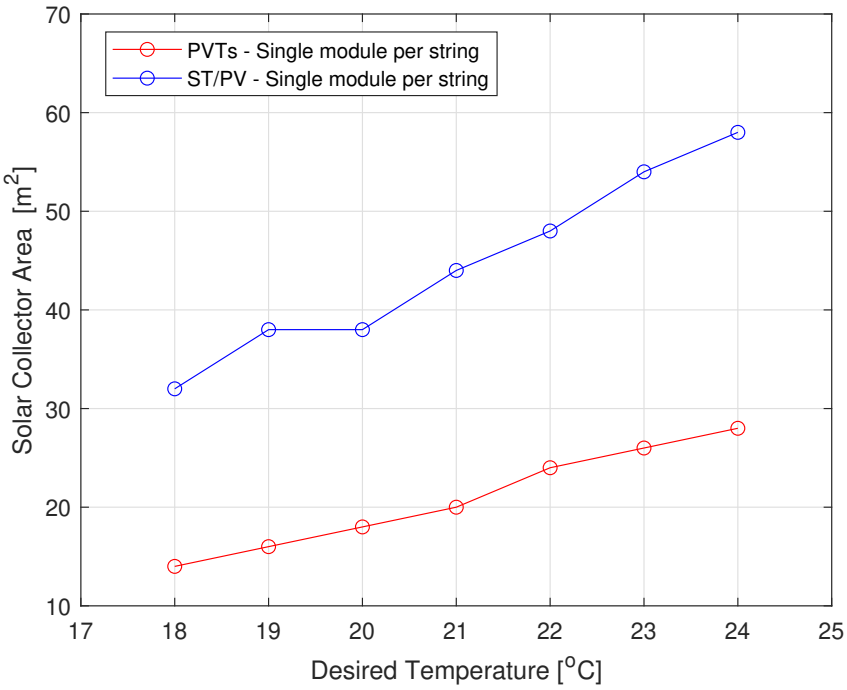

Figure 4.10: Required solar collector area to achieve net thermal and net electrical consumption by considering several inside desired temperatures. [Estimated in the City of Delft was considered with water-based PVT modules of 2.0 m^2 with no tilt angle. STs/PVs Type: ST modules for heating and PV modules for electricity.]

4.3 Conclusions

The sensitivity analysis provides detailed insights into its behavior by evaluating various parameters such as building thermal characteristics, solar module configuration, and occupant behavior. Two scenarios are explored for building thermal insulation: ADR and NZEB insulation. Additionally, the analysis considers two building typologies detached houses and mid-row terraced buildings with different configurations of PVT, PV, and ST modules, including series and parallel setups.

The study reveals that the space heating demand per unit area stabilizes as the number of stories in a building increases, regardless of insulation quality. This stabilization is attributed to the reduced influence of top apartments with higher heat requirements on middle apartments. However, the total heat demand per area differs between insulation scenarios. Moreover, the analysis shows a linear relationship between the apartment floor area and heating demand, with detached buildings exhibiting higher thermal demands due to greater exposure to the environment. The desired indoor temperature significantly affects space heating consumption, with higher temperatures leading to nearly double the heating demand.

The configuration and sizing of solar collectors are crucial in meeting space heating demands. The only PVT configuration and PVT/PV configuration were found more space-efficient than the ST/PV setup, requiring fewer modules to achieve net energy exchange. Adding more PVT modules per string only marginally increases during winter, highlighting the importance of seasonal heat storage. ST modules outperform PVT modules in heat production, particularly during high irradiance periods. The required solar collector area for maintaining desired indoor temperatures varies significantly, emphasizing the need for flexibility in design to accommodate different occupant behaviors.

Chapter 5

Amsterdam Building Analysis

After studying the sensitivity of the integrated system across various housing types and conditions, the analysis will focus on several existing mid-row buildings in Amsterdam. One primary objective was to size and determine the required PVT, ST, or PV modules for each building while examining the feasibility of utilizing these technologies for both space heating and domestic hot water. To achieve this goal, the Amsterdam Institute for Advanced Metropolitan Solutions (AMS Institute) provided heat demand data for both space heating and domestic hot water for several buildings in Amsterdam.

5.1 Typical Amsterdam building case

From a database of the AMS Institute, five buildings with similar sizes and geometries in Amsterdam were selected for analysis to determine the optimal system size under ideal conditions (no shading conditions) to fulfill both household thermal demand and heat pump electrical demand. Initially, a detailed examination of one of these buildings was carried out, followed by an analysis covering all selected cases. The annual heat demand for space heating and domestic hot water of the chosen buildings, along with other key characteristics, are presented in Table 5.1. This data is represented in the AMS data under two scenarios: one with the existing insulation of the buildings, which directly affects the demand for space heating, and the other scenario representing a renovation with new insulation. This renovation decreases space heating demand by at least 40% in all buildings.

Table 5.1: Building characteristics and thermal demand over selected buildings in Amsterdam.

Building	Roof Area	W/F	DHW	SH	
				Current Insulation	New Insulation
B1	142	3/4	10,825	61,579	18,724
B2	163	3/3	13,200	19,880	11,450
B3	158	3/5	29,023	43,710	25,176
B4	134	2/4	32,794	49,390	28,447
B5	69	2/4	6,841	31,332	18,597

B1: Beursstraat 25 built on 1700. B2: Warmoesstraat 96 built on 1693. B3: Beursstraat 21 built on unknown date. B4: Beursstraat 5 built on 1748. B5: Oudebrugsteeg 3 built on 1685. W/F: "W" represents the amount of windows per floor and "F" represents the amount of floors per building. Roof area units in m2. DHW units in kWh. SH units in kWh.

5.1.1 Detail case of Beursstraat 25

A detailed case study of one of the selected buildings is closely examined due to its higher heat demand among the selected structures. This mid-row residential building, highlighted in Figure 5.1a, is located at Beursstraat 25 (1012 JV, Amsterdam). The building, originally constructed in 1807, has four stories and a roof area of 142 m^2. Potential renovations could lead to a significant reduction of up to 70% in the building's total space heating demand, as outlined in Table 5.1. The difference in space heating demand is visualized in Figure 5.1b, showing a decrease in heating demand in the renovated scenario.

(a) Beursstraat 25 building

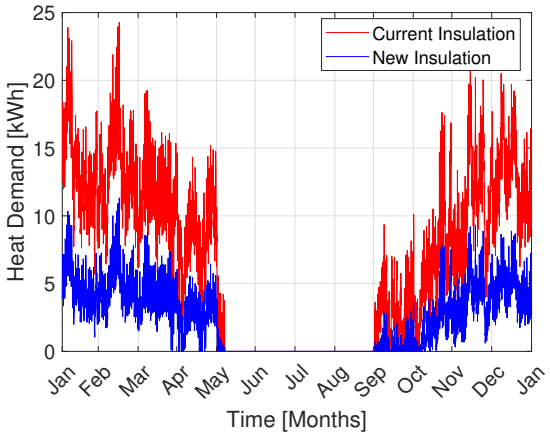

(b) SH contribution in Beursstraat 25.

Figure 5.1: Comparison of space heating consumption before and after building renovation: case study of Beursstraat 25, Amsterdam. (a) Aerial image that provides a view of Beursstraat 25 (1012 JV, Amsterdam), a residential building constructed in 1807 (Google, n.d.). [Contours of the building are highlighted in yellow] (b) Space heating consumption in the cases of using the current insulation and a new insulation obtained through a building renovation.

In contrast to space heating, the DHW demand is not reduced through the use of new insulation. For the Beursstraat 25 building, the weekly average DHW heat demand is depicted in Figure 5.2a. The weekly average heat demand exhibits a sinusoidal pattern throughout the year, peaking during the winter months and reaching a minimum in the summer months. A closer examination of the first week of the year reveals DHW heat consumption patterns, as illustrated in Figure 5.2b, where two peak consumption periods occur each day: the first in the morning and the second at the end of the day.

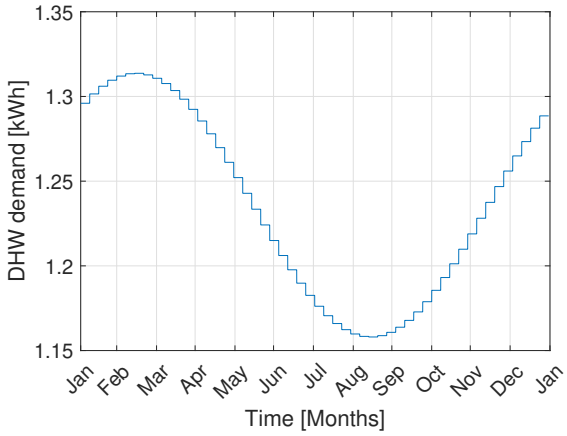

(a) Weekly average DHW heat demand during the year.

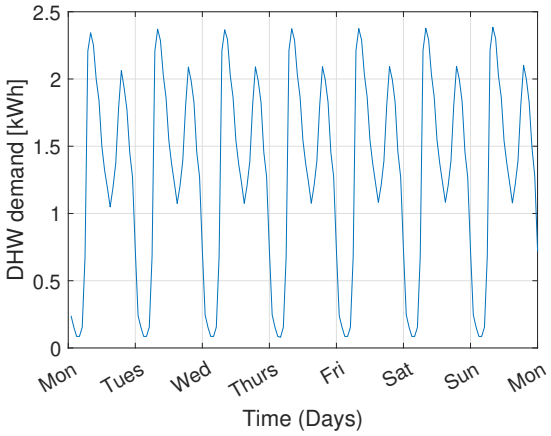

(b) DHW demand in the first week of the year.

Figure 5.2: Domestic Hot Water Heat Demand Variations at Beursstraat 25, Amsterdam. (a) Weekly average DHW heat demand in Beursstraat 25 over the whole year. (b) DHW heat hourly demand during the first week of the year in Beursstraat 25.

Therefore, to effectively supply both space heating demand and domestic hot water demand at Beursstraat 25, the influence of the heat pump is analyzed. As depicted in Figure 5.3a, the effectiveness of meeting the entire heat demand heavily depends on the maximum source mass flow rate that supplies the heat pump. This source mass flow rate consists of the flow from PVT modules, ST modules, or the ATES system, which provides the heat to be enhanced. The results clearly indicate that higher heat demands necessitate a higher maximum source mass flow rate, as illustrated in Figure 5.3b. This relationship highlights the importance of addressing a higher maximum source mass flow rate for substantial heat demands. As shown in Figure 5.3a, the necessary maximum source mass flow rate for SH demand should be around 0.6 kg/s and 0.3 kg/s for the current insulation and new insulation scenarios, respectively, in the Beursstraat 25 building.

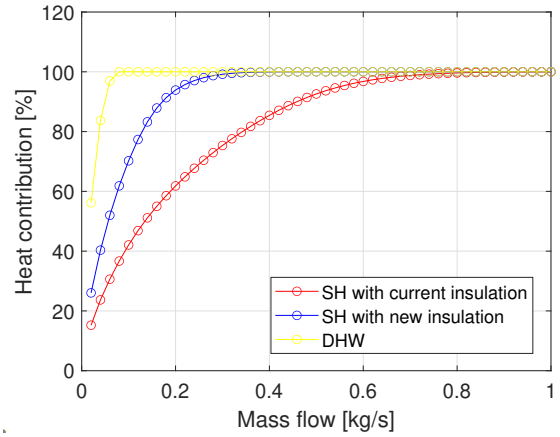

(a) Possible HP heat contribution by changing the maximum source mass flow.

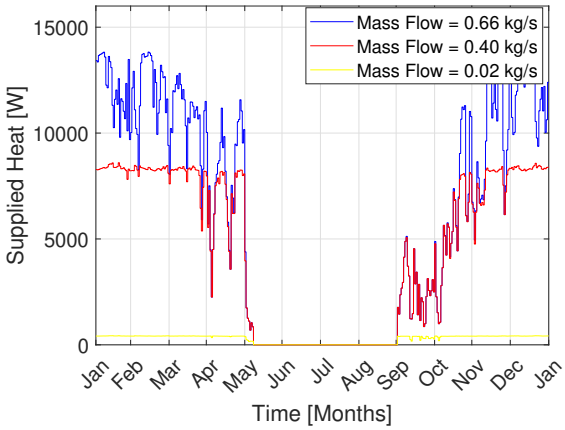

(b) Heat supply by changing the maximum source mass flow.

Figure 5.3: Effect of Maximum Source Mass Flow Rate on Heat Pump Contribution and Space Heating in Beursstraat 25, Amsterdam. (a) Heat contribution by changing the maximum source mass flows rate that provides heat to the heat pump at a constant $10°C$ in different heat demand over the building in the Beursstraat 25 (b) Space heating provided by the heat pump at three different maximum source mass flow rates at the building Beursstraat 25 by using the current insulation.

Solar collector system sizing

To supply enough heat at Beursstraat 25, the impact of a number of modules per string is evaluated as shown in Figure 5.4a and Figure 5.4b. Figure 5.4a indicates that using two modules per string provides an improvement in thermal performance for the PVT system and a reduction in the thermal mismatch with fewer strings compared to the case of using a single module per string. However, adding more modules per string would no longer made a relevant improvement on the thermal behavior of the module string. Moreover, the thermal mismatch considering the total number of modules is shown in Figure 5.4b. Results evident that if a single module per string configuration is considered, a lower amount of modules is required to achieve net thermal conditions compared to other configurations with more modules per string. This situation occurs due to the significant thermal impact of the mass flow rate, over the relatively small temperature increase of adding more modules per string.

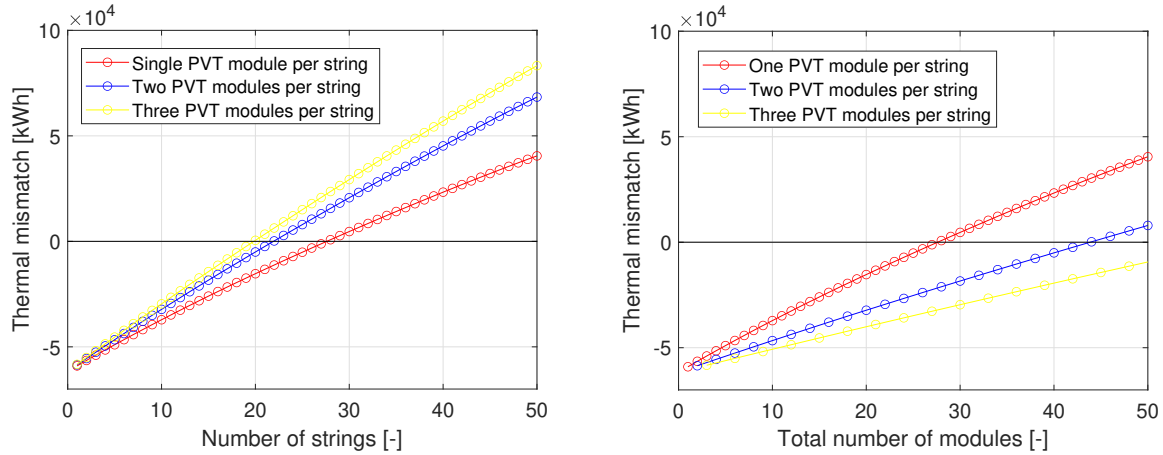

(a) SH thermal mismatch in Beursstraat 25 with current insulation.

(b) SH thermal mismatch in Beursstraat 25 with current insulation.

Figure 5.4: Thermal mismatch between the heat produced by the PVT system and the space heating demand using an ATES system on the Beursstraat 25 building: comparison of string and total module configurations. (a) Thermal mismatch between the heat produced by the PVT system and the space heating demand while using an ATES system on the Beursstraat 25 building in function of the amount of strings of the PVT system. (b) Thermal mismatch between the heat produced by the PVT system and the space heating demand while using an ATES system on the Beursstraat 25 building in function of the total amount of modules.

Meanwhile, the influence of the PVT modules per string on the heat pump's electrical demand is also considered. Increasing the number of strings raises electrical consumption due to the higher mass flow rate passing through the heat pump. As shown in Figure 5.5a, increasing the number of modules per string reduces the number of strings needed to achieve a net zero electrical mismatch. Furthermore, Figure 5.5b indicates that configurations with fewer PVT modules per string require more strings to generate enough electricity to offset the heat pump's consumption, contrary to the thermal mismatch behavior. This suggests that configurations with a higher number of modules per string are more suitable for optimizing the building's roof space.

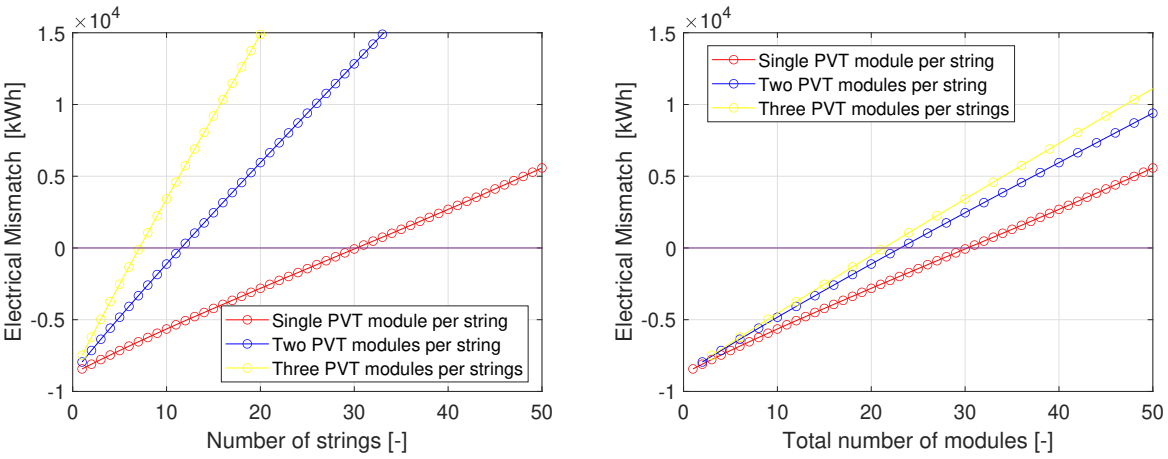

(a) SH electrical mismatch in Beursstraat 25 with current insulation.

(b) SH electrical mismatch in Beursstraat 25 with current insulation.

Figure 5.5: Overall electrical mismatch between PVT production and the heat pumps consumption considering the number of modules per string and total number of strings in the Beursstraat 25 building. (a) Overall electrical mismatch between the electrical consumption of the heat pumps and the electricity produced by PVT modules by considering several modules per string in function of the total number of strings in the Beursstraat 25 building. (b) Overall electrical mismatch between the electrical consumption of the heat pumps and the electricity produced by the PVT modules by considering the total number of modules in the Beursstraat 25 building.

Solar module configuration

Analysis of the case of Beursstraat 25 gives insights into which solar collector configuration would perform best under the current insulation conditions for the space heating supply. From Table 5.2, the PVT/PV configuration is analyzed and proves that a single module per string configuration has the best results in taking up the least coverage on the roof. In a mid-row four story building, the PVT/PV and the only PVT systems utilize almost 40% of the building's roof area, far less than using the ST/PV configuration with 110% of roof coverage. Furthermore, placing two modules in each string increases the total roof area required for net energy exchange as compared to using one module in each string. This suggests that more modules will be required to obtain the equivalent thermal exchange, whereas the net electrical exchange would require less. Despite this, the configuration that proves most efficient in terms of roof coverage remains a single PVT module per string.

Table 5.2: System sizing for Beursstraat 25 considering current insulation for the space heating demand, by taking into account three configurations.

		Current				
Modules per string	Type	Net Thermal	Net Electrical	Total	Area	Roof Coverage
1	PVTs	28	31	31	62	44
	STs/PVs	25	41	66	132	93
	PVTs/PVs	28	2	30	60	42
2	PVTs	44	24	44	88	62
	STs/PVs	36	40	80	160	113
	PVTs/PVs	44	0	44	88	62

PVTs Type: Only PVT modules in the configuration. STs/PVs Type: ST modules for heating and PV modules for electricity. PVTs/PVs Type: PVT modules for heating together with a contribution to the electrical demand that is fulfilled by PV modules. Area units in m^2. Roof Coverage units in %. ATES used as long term storage.

In contrast with Table 5.2, Table 5.3 considers the renovated insulation instead of the current one. Table 5.3 highlights that the most roof space efficient configuration is a single PVT module per string. However, in contrast to the previous case, the difference in roof coverage from this optimal configuration is not significantly different from other configurations. In all cases, with the new insulation, the required roof coverage is 20% of the solar collector area in the current case scenario.

Table 5.3: System sizing for Beursstraat 25 considering renovated insulation for the space heating demand, by taking into account three configurations.

		Renovated				
Modules per string	Type	Net Thermal	Net Electrical	Total	Area	Roof Coverage
1	PVTs	9	10	10	20	14
	STs/PVs	8	13	21	42	30
	PVTs/PVs	9	1	10	20	14
2	PVTs	14	8	14	28	20
	STs/PVs	12	14	26	52	37
	PVTs/PVs	14	0	14	28	20

PVTs Type: Only PVT modules in the configuration. STs/PVs Type: ST modules for heating and PV modules for electricity. PVTs/PVs Type: PVT modules for heating together with a contribution to the electrical demand that is fulfilled by PV modules. Area units in m^2. Roof Coverage units in %. ATES used as long term storage.

For the case of DHW at Beursstraat 25, the number of required modules is shown in Table 5.4. For all cases, the required modules for achieving net electrical demand is much higher than the required ones for net thermal conditions. This occurs because more energy is needed from the heat pumps to heat water to $60°C$ compared to temperature requirements for space heating which usually are between $30°C$ and $40°C$. In this case, the only PVT and PVT/PV configurations provide similar results, that are considerably lower than the ST/PV configuration.

Table 5.4: System sizing for Beursstraat 25 domestic hot water, by taking into account three configurations.

		DHW				
Modules per string	Type	Net Thermal	Net Electrical	Total	Area	Roof Coverage
1	PVTs	4	13	13	26	18
	STs/PVs	4	14	18	36	25
	PVTs/PVs	4	8	12	24	17
2	PVTs	8	12	12	24	17
	STs/PVs	6	14	20	40	28
	PVTs/PVs	8	3	11	22	15

PVTs Type: Only PVT modules in the configuration. STs/PVs Type: ST modules for heating and PV modules for electricity. PVTs/PVs Type: PVT modules for heating together with a contribution to the electrical demand that is fulfilled by PV modules. Area units in m^2. Roof Coverage units in %. ATES used as long term storage.

Heat pump electrical consumption variance

The variance of the heat pump's electrical consumption is analyzed by considering the influence of increasing the number of strings using Equation 5.1 with the HP electrical consumption (W^{HP}), as shown in Figure 5.6a and Figure 5.6b for ADR and NZEB insulation, respectively. Both figures indicate that changing the number of strings, which represents the mass flow entering the heat pump, significantly impacts the heat pump's electrical consumption. The variance,

taking into account the annual mean heat pump electrical demand, reveals a clear minimum at a low amount of strings, which closely coincides with the necessary amount of PVTs to achieve both net thermal and net electrical consumption.

$$r = \frac{\sqrt{\sum_{i=1}^{n}(W^{HP} - \overline{W^{HP}})^2}}{\overline{W^{HP}}} \tag{5.1}$$

Figure 5.7a and Figure 5.7b depict the variation in heat pump electrical consumption by comparing the use of one PVT module to 27 PVT modules, respectively. It is evident that electrical consumption rises as the number of PVT modules increases, particularly during summer months, attributable to greater heat injection into the hot aquifer of the ATES system. This increased heat injection necessitates greater electricity usage for the heat pumps. In both scenarios, the overall pattern of heat pump electricity consumption exhibits a sinusoidal trend. But closer to the constant mean value, in the case of using 27 PVT modules.

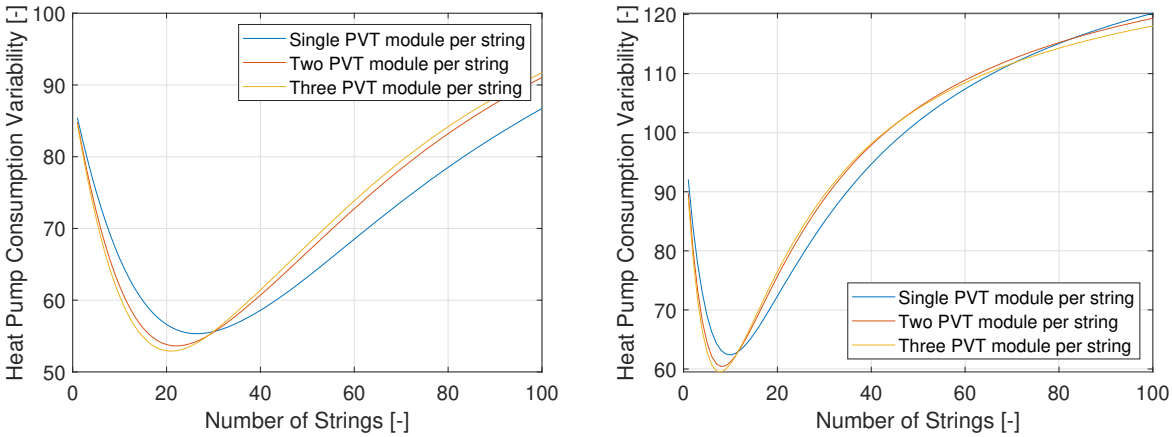

(a) HP consumption profile variability using the current insulation.

(b) HP consumption profile variability using the new insulation.

Figure 5.6: Overall heat pump electrical consumption variability of the whole system in function of the used PVT strings for the Beursstraat 25 building. (a) HP consumption profile variability using the current insulation. (b) HP consumption profile variability using the new insulation.

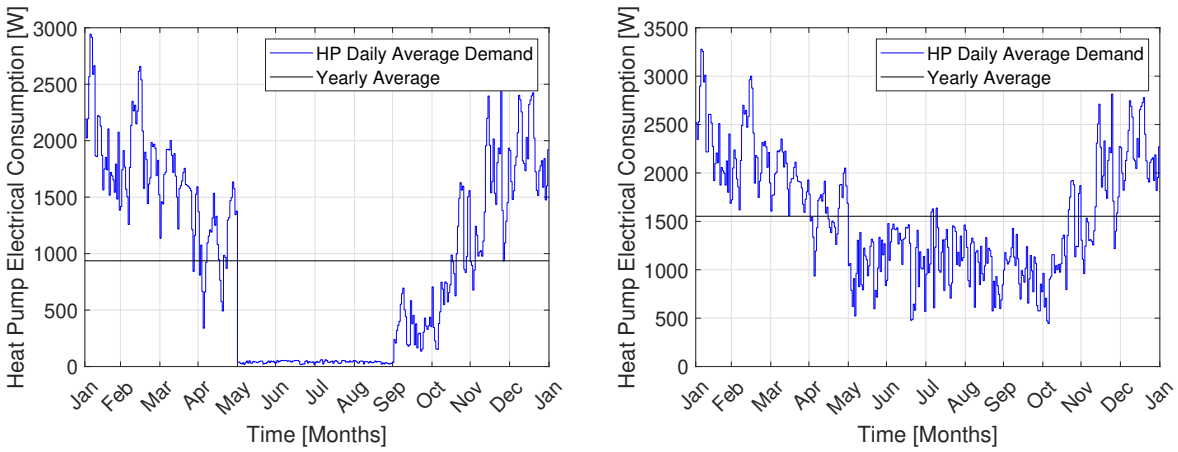

(a) HP consumption profile using 1 PVT module.

(b) HP consumption profile using 27 PVT modules.

Figure 5.7: Overall HP electrical consumption of the whole system in function of the used PVT strings for the Beursstraat 25 building. (a) HP consumption profile variability using the current insulation. (b) HP consumption profile variability using the new insulation.

Irradiance Control

By considering an irradiance control mechanism that switches between Summer mode and Spring mode, rather than a heating system that sequentially transitions from Summer mode directly to Sping mode, the system's performance can be analyzed in terms of irradiance. This control regime, based on an irradiance threshold G, operates such that for irradiance values higher than G, the heating system will function using Summer mode and Winter mode. In the other hand, for irradiance values equal to or lower than G, the heating system will operate using Spring mode and Winter mode. This configuration allows us to determine if using an irradiance-based control system can improve the overall system efficiency.

Figure 5.8 illustrates the number of PVT modules required to achieve net energy balance within the described control system for Beursstraat 25, in the case of considering the current insulation. It is evident that by adjusting the irradiance criteria, the required number of modules saturates. This saturation indicates that Summer mode is not optimal, while Spring mode and Winter mode are meeting the entire heat demand. By increasing the utilization of the Spring mode, results in an improvement in heat efficiency. This suggests that incorporating a heat pump can enhance the overall energy efficiency of the system more effectively than relying on Summer mode.

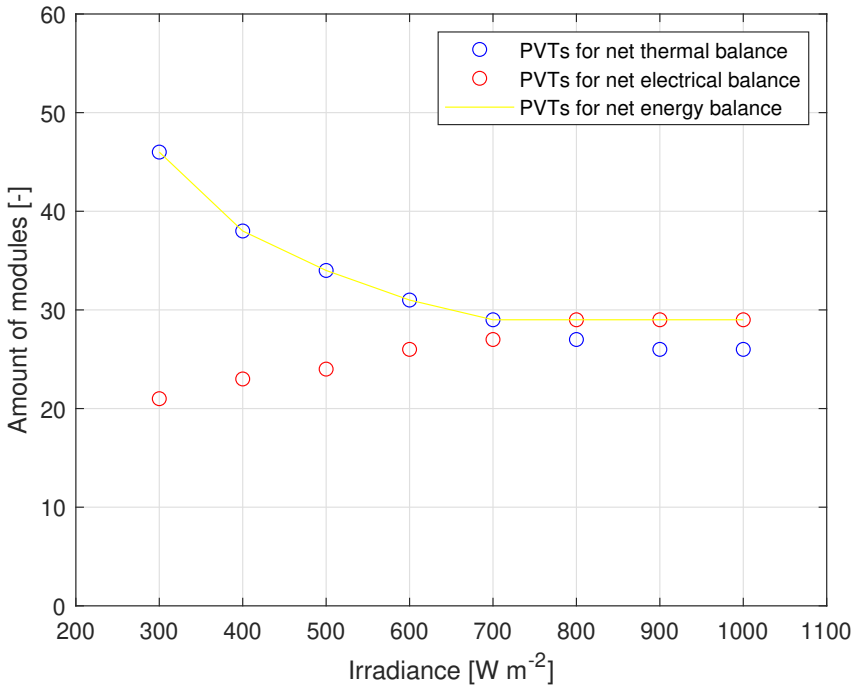

Figure 5.8: Required solar collector area to achieve net thermal and net electrical exchange by considering several inside desired temperatures. [Estimated in the City of Delft was considered with water-based PVT modules of 2.0 m^2 with no tilt angle.]

5.1.2 Complete building cases and operational modes

Beursstraat 25, along with the other selected buildings, are discussed in this section in a general manner. All scenarios use significantly fewer PVT and PV modules with the PVT/PV configuration for both net thermal and net electrical annual exchange equally for current and renovated scenarios, as illustrated in Table 5.5, compared to those that use only PVT modules or the ST/PV configuration. In addition, the ATES system works as seasonal storage in all scenarios.

Table 5.5: Required modules to achieve net thermal and electrical annual exchange at different buildings in Amsterdam. By taking into several configurations of solar modules, by considering both current and renovated thermal conditions. An ATES system is used as long term heat storage.

Building	Current			Renovated		
	PVTs	STs/PVs	PVT/PVs	PVTs	STs/PVs	PVT/PVs
B1	31	66	30	10	21	10
B2	11	24	11	7	14	7
B3	24	51	23	14	30	14
B4	27	56	26	16	34	16
B5	16	35	16	10	22	10

B1: Beursstraat 25 built on 1700. B2: Warmoesstraat 96 built on 1693. B3: Beursstraat 21 built on unknown date. B4: Beursstraat 5 built on 1748. B5: Oudebrugsteeg 3 built on 1685. PVTs Type: Only PVT modules in the configuration. STs/PVs Type: ST modules for heating and PV modules for electricity. PVTs/PVs Type: PVT modules for heating together with a contribution to the electrical demand that is fulfilled by PV modules. All modules possess an area of 2 m^2. A single PVT or ST module is used per string in these cases. An ATES system is used for long-term storage.

For the DHW heat demand in the selected buildings, the required modules to achieve annual net heat and electrical exchange are shown in Table 5.6. Similar to the space heating demand cases, the optimal configuration to minimize roof coverage is the PVT/PV configuration, but the only PVT configuration closely aligns with the PVT/PV due to the high efficiency that the PVT modules brings into the system.

Table 5.6: Required modules to achieve both thermal and electrical demand of the DHW demand at different buildings in Amsterdam. By taking into several configurations of solar modules.

Selected Buildings	DHW		
	Only PVTs	STs/PVs	PVT/PVs
B1	13	18	12
B2	17	21	15
B3	36	43	33
B4	41	50	37
B5	9	12	8

B1: Beursstraat 25 built on 1700. B2: Warmoesstraat 96 built on 1693. B3: Beursstraat 21 built on unknown date. B4: Beursstraat 5 built on 1748. B5: Oudebrugsteeg 3 built on 1685. PVTs Type: Only PVT modules in the configuration. STs/PVs Type: ST modules for heating and PV modules for electricity. PVTs/PVs Type: PVT modules for heating together with a contribution to the electrical demand that is fulfilled by PV modules. A single PVT or ST module is used per string in these cases. ATES used as long term storage.

Meanwhile, the space heating contribution using the optimal configuration (PVT/PV configuration) described previously is depicted in Table 5.5. Across all cases, the direct heat provided from the solar PVT modules to space heating in Summer mode accounts for less than 10% of the total supply, as shown in Table 5.7. Appendix A.1 shows the operational conditions of Summer mode, from which is clear that only in a few moments is possible to provide peak power demand.

In contrast, the primary heat supply mode of the whole system involves using PVT modules coupled to the heat pump, contributing around 67% of the supply in all cases, as shown in Table 5.7. The heat pump size of the Spring mode varies around 2-4 kW and 1-2 kW per building floor for the current case and the renovated case, respectively. In Appendix A.2, the operational conditions of the heat pump at the Beursstraat 25 building are analyzed. In which is presented how Spring mode mostly operates with an inlet water temperature in the PVT system of $10°C$. Although the system also operates at higher inlet temperatures, these instances are less frequent.

Additionally, Winter mode operates mostly during the peak winter loads when higher heat loads are required and Summer mode or Spring mode are not enough to cover the entire heat demand. Table 5.7 shows that the heat contribution of Winter mode is around 30% in all cases. Meanwhile, the heat pump size of Winter mode varies around 2-5 kW per building floor. Appendix A.3 indicates that this operational mode covers a few moments of high peak demand.

Table 5.7: Thermal contribution for the space heating demand required at each building in Amsterdam, taking into account the three thermal contributions modes.

Building Address	Current			Renovated		
	Mode 1	Mode 2	Mode 3	Mode 1	Mode 2	Mode 3
B1	7.3	69.4	23.3	3.4	66.8	29.8
B2	4.1	67.4	28.5	2.6	66.4	31.0
B3	4.1	67.5	28.4	2.6	66.0	31.4
B4	4.1	66.4	29.5	2.6	66.6	30.8
B5	5.3	69.1	25.6	4.2	67.7	28.1

B1: Beursstraat 25 built on 1700. B2: Warmoesstraat 96 built on 1693. B3: Beursstraat 21 built on unknown date. B4: Beursstraat 5 built on 1748. B5: Oudebrugsteeg 3 built on 1685. Mode 1: Heat provided by PVT/ST modules directly to the space heating demand through heat exchangers. Mode 2: Heat provided by the coupled PVT/ST with HP to the space heating demand. Mode 3: Heat provided by the ATES system with a heat pump to supply the space heating demand. A single PVT or ST module is used per string in these cases. All modes unit in %.

5.2 Conclusions

The analysis focused on mid-row buildings in Amsterdam to assess the feasibility of integrating PVT, ST, or PV modules for space heating and domestic hot water supply. Both current insulation conditions and a renovated scenario with improved insulation were examined, which could potentially reduce space heating demand by up to 70%.

The number of modules per string and the type of solar collector significantly affect the thermal and electrical performance in the sizing of the solar collector system. Different configurations (PVTs, STs/PVs, PVTs/PVs) yield varying results in terms of required modules, area coverage, and net thermal/electrical exchange. Among these, the PVT/PV configuration with one module per string emerged as the optimal solution, presenting almost identical results to using only PVT modules. This configuration required less roof coverage while achieving an effective net thermal and electrical balance.

Meeting the heat demand heavily depended on the maximum source mass flow rate that supplies the heat pump. Higher heat demands necessitats a higher maximum source mass flow rate. The optimal source mass flow rates for SH demand were around 0.6 kg/s and 0.3 kg/s for the current insulation and new insulation scenarios, respectively. The electrical consumption behavior of the heat pumps aligned with the shape of the heat demand. Increasing the number of strings significantly impacted the heat pump's electrical consumption, with a clear minimum electrical demand at a low number of strings.

For space heating supply, the optimal configuration to minimize roof coverage involved using a single PVT module per string. In contrast, using two modules per string required more roof coverage but achieved net thermal exchange with fewer strings. For DHW, configurations with only PVT or PVT/PV modules were more efficient than ST/PV configurations. The primary heat supply mode involved using PVT modules coupled to the heat pump, contributing around 67% of the supply. Winter mode, representing the ATES-HP coupling contribution, was crucial for meeting peak winter loads. Also, implementing an irradiance-based control system improved the overall system efficiency. The system's performance showed saturation in required module numbers, indicating that higher utilization of Spring mode enhanced thermal efficiency.

These trends were consistent across all buildings, indicating that optimal configurations typically involve PVT/PV modules for both space heating and DHW. Notably, DHW demand requires fewer modules compared to space heating. In terms of heat operational modes, the total contribution to space heating demand from the summer mode is less than 10%, while the spring mode contributes 60%, and the winter mode accounts for the remaining 30%.

Chapter 6

Final Conclusions and Recommendations

This thesis presents an analysis of space heating demand and the integration of solar thermal technologies to meet this demand in residential buildings. The developed space heating model, implemented in the PVMD Toolbox, is user-friendly and adaptable, requiring only general building characteristics to simulate thermal demand in various household types. It accurately estimates heat demand based on building geometry and thermal properties, making it a valuable tool for energy management.

By integrating the heat demand model with other models of system components, several operational modes were considered to meet thermal and energy requirements throughout the year. These modes ensure that each component, including necessary temperatures for various thermal applications, is adequately addressed. The sensitivity analysis offers detailed insights by evaluating parameters such as building thermal characteristics, solar module configuration, and occupant behavior. Two insulation scenarios, ADR and NZEB, along with different building typologies, were explored, revealing that space heating demand per unit area stabilizes with an increasing number of stories. However, the total heat demand per area varies between insulation scenarios. Detached buildings exhibit higher thermal demands due to greater environmental exposure, and the desired indoor temperature significantly affects space heating consumption.

The study emphasizes the critical role of solar collector configuration and sizing in meeting space heating demands. The PVT and PVT/PV configurations were found to be more space-efficient than the ST/PV setup, requiring fewer modules to achieve net energy exchange. Seasonal heat storage is essential as adding more PVT modules per string only marginally improves temperature during winter. ST modules outperform PVT modules in heat production during high irradiance periods. However, while using PVT modules, the required solar collector area is reduced. Which is provides flexibility to the system design if the considered heat demand varies significantly due to unexpected occupant behaviors.

An analysis of mid-row buildings in Amsterdam assessed the feasibility of integrating PVT, ST, or PV modules for space heating and domestic hot water supply. Both current insulation conditions and a renovated scenario with improved insulation were examined, with the latter potentially reducing space heating demand by up to 40%. The study found that the number of modules per string and the type of solar collector significantly affect thermal and electrical performance. Among different configurations, the PVT/PV setup with one module per string emerged as the optimal solution, offering effective net thermal and electrical balance with less roof coverage.

The observed trends were consistent across all buildings, indicating that optimal configurations typically involve PVT/PV modules for both space heating and DHW. Notably, DHW demand requires fewer modules than space heating. In terms of heat operational modes, the total contribution to space heating demand from the Summer mode is less than 10%, while the Spring mode contributes around 60%, and the Winter mode accounts for the remaining 30%.

In conclusion, this thesis demonstrates that integrating solar thermal technologies with effective building insulation can significantly reduce space heating demands and improve energy efficiency in residential buildings. The findings provide valuable insights for optimizing solar collector configurations and highlight the importance of flexible and adaptive energy management strategies to meet diverse household energy needs.

Recommendations

Throughout the development of this thesis project, several assumptions and potential research topics emerged. However, due to the limited scope of this project, it was not possible to explore all of these topics in depth. Therefore, here are some recommendations for further investigation on various related subjects

- Future research for this project could involve analyzing various types of PV, PVT, and ST modules to determine the optimal solar technology for improving system sizing and efficiency, together with the use of more complete models that take into account more dynamic effects in the electrical and thermal efficiencies, for the heat exchanger and the solar modules. Comparative studies could focus on factors such as energy production, durability, and cost-effectiveness to identify the most suitable technologies for building application considering The Netherlands weather conditions.

- In the case of the space heating validation, the annual heat consumption was validated, and hourly comparison was not made, due to the difficulty of finding complete cases with hourly data. Therefore, a the use of hourly profiles could be utilized in a more complete validation for the space heating model.

- Additionally, conducting an economic analysis of the entire system beyond technical feasibility would be beneficial. This analysis should assess the economic viability of integrating solar collectors with heat pumps, including life-cycle costs, payback periods, and potential energy savings.

- Furthermore, investigating the optimal sizing and economic feasibility of Aquifer Thermal Energy Storage systems is recommended. This includes analyzing installation and operational costs across different building thermal conditions. Understanding the scalability and minimum building requirements for economic viability would be essential for broader implementation in urban environments. Together with a study of the optimal temperatures for the hot and cool aquifer. In this way, by increasing the temperature of the hot aquifer, the COP of the heat pump increases, which will reduce the peak electrical consumption during winter peaks which could prevent power grid congestion in urban areas.

References

Ahmad, L., Khordehgah, N., Malinauskaite, J., & Jouhara, H. (2020). Recent advances and applications of solar photovoltaics and thermal technologies. *Energy*, *207*, 118254. doi: https://doi.org/10.1016/j.energy.2020.118254

Ahmadi, A., Ehyaei, M., Doustgani, A., Assad, M. E. H., Hmida, A., Jamali, D., ... Razmjoo, A. (2021). Recent residential applications of low-temperature solar collector. *Journal of Cleaner Production*, *279*, 123549. doi: https://doi.org/10.1016/j.jclepro.2020.123549

Ampatzi, E., Knight, I., & Wiltshire, R. (2013). The potential contribution of solar thermal collection and storage systems to meeting the energy requirements of north european housing. *Solar energy*, *91*, 402–421. doi: https://doi.org/10.1016/j.solener.2012.09.008

Angenendt, G., Zurmühlen, S., Rücker, F., Axelsen, H., & Sauer, D. U. (2019). Optimization and operation of integrated homes with photovoltaic battery energy storage systems and power-to-heat coupling. *Energy Conversion and Management: X*, *1*, 100005. doi: https://doi.org/10.1016/j.ecmx.2019.100005

Aydin, E., Kok, N., & Brounen, D. (2017). Energy efficiency and household behavior: the rebound effect in the residential sector. *The RAND Journal of Economics*, *48*(3), 749–782. doi: https://doi.org/10.1111/1756-2171.12190

Azevedo, J. A., Chapman, L., & Muller, C. L. (2016). Urban heat and residential electricity consumption: A preliminary study. *Applied Geography*, *70*, 59–67. doi: https://doi.org/10.1016/j.apgeog.2016.03.002

Barthelmes, V. M., Becchio, C., & Corgnati, S. P. (2016). Occupant behavior lifestyles in a residential nearly zero energy building: Effect on energy use and thermal comfort. *Science and Technology for the Built Environment*, *22*(7), 960–975. doi: https://doi.org/10.1080/23744731.2016.1197758

Beck, T., Kondziella, H., Huard, G., & Bruckner, T. (2016). Assessing the influence of the temporal resolution of electrical load and pv generation profiles on self-consumption and sizing of pv-battery systems. *Applied energy*, *173*, 331–342. doi: https://doi.org/10.1016/j.apenergy.2016.04.050

Behzadi, A., Arabkoohsar, A., & Yang, Y. (2020). Optimization and dynamic techno-economic analysis of a novel pvt-based smart building energy system. *Applied Thermal Engineering*, *181*, 115926. doi: https://doi.org/10.1016/j.applthermaleng.2020.115926

Belaïd, F. (2016). Understanding the spectrum of domestic energy consumption: Empirical evidence from france. *Energy Policy*, *92*, 220–233. doi: https://doi.org/10.1016/j.enpol.2016.02.015

Bellos, E., Tzivanidis, C., Moschos, K., & Antonopoulos, K. A. (2016). Energetic and financial evaluation of solar assisted heat pump space heating systems. *Energy conversion and management*, *120*, 306–319. doi: https://doi.org/10.1016/j.enconman.2016.05.004

Benda, V., & Černá, L. (2020). Pv cells and modules–state of the art, limits and trends. *Heliyon*, *6*(12). doi: https://doi.org/10.1016/j.heliyon.2020.e05666

Bergman, T. L., Lavine, A. S., Incropera, F. P., & DeWitt, D. P. (2007). *Fundamentals of heat and mass transfer* (6th ed.). Hoboken, NJ: John Wiley & Sons.

Bloemendal, M., Jaxa-Rozen, M., & Olsthoorn, T. (2018). Methods for planning of ates systems. *Applied Energy*, *216*, 534–557. doi: https://doi.org/10.1016/j.apenergy.2018.02.068

Carpino, C., Mora, D., Arcuri, N., & De Simone, M. (2017). Behavioral variables and occupancy patterns in the design and modeling of nearly zero energy buildings. In *Building simulation* (Vol. 10, pp. 875–888). doi: https://doi.org/10.1007/s12273-017-0371-2

Chaturvedi, S., Gagrani, V., & Abdel-Salam, T. (2014). Solar-assisted heat pump–a sustainable system for low-temperature water heating applications. *Energy Conversion and Management*, *77*, 550–557. doi: https://doi.org/10.1016/j.enconman.2013.09.050

Chow, T. T. (2018). A review on photovoltaic/thermal hybrid solar technology. *Renewable Energy*, Vol4_88–Vol4_119.

Cohen, R., & Khermouch, G. (2013). The giant headache that is net energy metering. *Electr. J*, *26*(6), 1–7.

Duijff, R., Bloemendal, M., & Bakker, M. (2023). Interaction effects between aquifer thermal energy storage systems. *Groundwater*, *61*(2), 173–182. doi: https://doi.org/10.1111/gwat.13163

D'oca, S., Fabi, V., Corgnati, S. P., & Andersen, R. K. (2014). Effect of thermostat and window opening occupant behavior models on energy use in homes. In *Building simulation* (Vol. 7, pp. 683–694). doi: https://doi.org/10.1007/s12273-014-0191-6

Energie Data Services Nederland (EDSN). (2014). *Average load profiles in the netherlands.* Retrieved from `http://www.edsn.nl/verbruiksprofielen/`

Eurostat. (n.d.). *Harmonized index of consumer prices: Electricity, gas, solid fuels and heat energy for netherlands [elgas0nlm086nest].* Retrieved from FRED, Federal Reserve Bank of St. Louis. Retrieved from `https://fred.stlouisfed.org/series/ELGAS0NLM086NEST` (Accessed on October 18, 2023)

Feldman, D., Ramasamy, V., Fu, R., Ramdas, A., Desai, J., & Margolis, R. (2021). *US solar photovoltaic system and energy storage cost benchmark (Q1 2020)* (Tech. Rep.). National Renewable Energy Lab.(NREL), Golden, CO (United States). doi: https://doi.org/10.2172/1764908

Fong, W.-K., Matsumoto, H., Lun, Y.-F., & Kimura, R. (2007). Influences of indirect lifestyle aspects and climate on household energy consumption. *Journal of Asian Architecture and Building Engineering*, *6*(2), 395–402. doi: https://doi.org/10.3130/jaabe.6.395

Fuentes, M. K. (1987). *A simplified thermal model for flat-plate photovoltaic arrays* (Tech. Rep.). Sandia National Labs., Albuquerque, NM (USA). Retrieved from `https://www.osti.gov/biblio/6802914`

Gilani, S., & O'Brien, W. (2018). Best practices guidebook on advanced occupant modelling. *Human Building Interaction Lab, Carleton University, Ottawa, Canada*. Retrieved from `https://carleton.ca/hbilab/wp-content/uploads/Best-Practices-Guidebook-on-Advanced-Occupant-Modelling.pdf`

Good, C., Andresen, I., & Hestnes, A. G. (2015). Solar energy for net zero energy buildings–a comparison between solar thermal, pv and photovoltaic–thermal (pv/t) systems. *Solar Energy*, *122*, 986–996.

Google. (n.d.). *Google earth location of beursstraat 25, 1012jv, amsterdam.* Retrieved from `https://earth.google.com/web/search/Beursstraat%2025/@52.37478968,4.89666083,0.78701433a,491.91472189d`

Grassi, W. (2017). *Heat pumps: fundamentals and applications.* Springer. doi: https://doi.org/10.1007/978-3-319-62199-9

Gueymard, C., et al. (1995). *Smarts2: a simple model of the atmospheric radiative transfer of sunshine: algorithms and performance assessment* (Vol. 1). Florida Solar Energy Center Cocoa, FL. Retrieved from `https://ww.instesre.org/GCCE/SMARTS2.pdf`

Hayn, M., Bertsch, V., & Fichtner, W. (2014). Electricity load profiles in europe: The importance of household segmentation. *Energy Research & Social Science*, *3*, 30–45. Retrieved from `https://doi.org/10.1016/j.erss.2014.07.002`

Herrando, M., Markides, C. N., & Hellgardt, K. (2014). A uk-based assessment of hybrid pv and solar-thermal systems for domestic heating and power: System performance. *Applied Energy*, *122*, 288–309. doi: https://doi.org/10.1016/j.apenergy.2014.01.061

Herrando, M., Wang, K., Huang, G., Otanicar, T., Mousa, O. B., Agathokleous, R. A., ... others (2023). A review of solar hybrid photovoltaic-thermal (pv-t) collectors and systems. *Progress in Energy and Combustion Science*, *97*, 101072. doi: https://doi.org/10.1016/j.pecs.2023.101072

International Commission on Illumination (CIE). (1973). Standardization of luminous distribution on clear skies. In *International conference on illumination.* (CIE Publication No. 22, Paris)

International Energy Agency (IEA). (2022). *IEA Energy and Carbon Tracker 2022.* Retrieved 2023-09-29, from `https://www.iea.org/data-and-statistics/data-product/iea-energy-and-carbon-tracker-2022`

International Renewable Energy Agency (IRENA). (2015). *Renewable energy statistics 2015.* Abu Dhabi. Retrieved from `https://www.irena.org/Publications/2015/Jun/Renewable-Energy-Capacity-Statistics-2015`

International Renewable Energy Agency (IRENA). (2023). *Renewable energy statistics 2023.* Abu Dhabi. Retrieved from `https://www.irena.org/Publications/2023/Jul/Renewable-Energy-Statistics-2023`

Khani, M., Baneshi, M., & Eslami, M. (2019). Bi-objective optimization of photovoltaic-thermal (pv/t) solar collectors according to various weather conditions using genetic algorithm: A numerical modeling. *Energy*, *189*, 116223. doi: https://doi.org/10.1016/j.energy.2019.116223

Kim, J.-H., Kim, J.-T., et al. (2012). Comparison of electrical and thermal performances of glazed and unglazed pvt collectors. *International Journal of Photoenergy*, *2012*. doi: https://doi.org/10.1155/2012/957847

Kowsari, R., & Zerriffi, H. (2011). Three dimensional energy profile:: A conceptual framework for assessing household energy use. *Energy Policy*, *39*(12), 7505–7517. doi: https://doi.org/10.1016/j.enpol.2011.06.030

Linssen, J., Stenzel, P., & Fleer, J. (2017). Techno-economic analysis of photovoltaic battery systems and the influence of different consumer load profiles. *Applied Energy*, *185*, 2019–2025. doi: https://doi.org/10.1016/j.apenergy.2015.11.088

Majcen, D., Itard, L., & Visscher, H. (2013). Actual and theoretical gas consumption in dutch dwellings: What causes the differences? *Energy Policy*, *61*, 460–471. doi: https://doi.org/10.1016/j.enpol.2013.06.018

Martinopoulos, G. (2020). Are rooftop photovoltaic systems a sustainable solution for europe? a life cycle impact assessment and cost analysis. *Applied Energy*, *257*, 114035. doi: https://doi.org/10.1016/j.apenergy.2019.114035

Nieboer, N., & Filippidou, F. (2014). Inclusion of different energy performance levels for new buildings in national residential building typologies: Chapter 3.14 the netherlands. *Inclusion of New Buildings in Residential Building Typologies: Steps Towards NZEBs Exemplified for Different European Countries, 213-224, Darmstadt, Institut Wohnen und Umwelt GmbH. EPISCOPE Synthesis Report No. 1*. Retrieved from `http://resolver.tudelft.nl/uuid:d7ceb03f-699e-4db6-9638-d1db98f8f2f1`

Paatero, J. V., & Lund, P. D. (2006). A model for generating household electricity load profiles. *International journal of energy research*, *30*(5), 273–290. doi: https://doi.org/10.1002/er.1136

Perez, R., Seals, R., & Michalsky, J. (1993). All-weather model for sky luminance distribution—preliminary configuration and validation. *Solar energy*, *50*(3), 235–245. doi: https://doi.org/10.1016/0038-092X(93)90017-I

Porse, E., Derenski, J., Gustafson, H., Elizabeth, Z., & Pincetl, S. (2016). Structural, geographic, and social factors in urban building energy use: Analysis of aggregated account-level consumption data in a megacity. *Energy Policy*, *96*, 179–192. doi: https://doi.org/10.1016/j.enpol.2016.06.002

Richter, A., Hermle, M., & Glunz, S. W. (2013). Reassessment of the limiting efficiency for crystalline silicon solar cells. *IEEE journal of photovoltaics*, *3*(4), 1184–1191. doi: https://doi.org/10.1109/JPHOTOV.2013.2270351

Ruhnau, O., Hirth, L., & Praktiknjo, A. (2019). Time series of heat demand and heat pump efficiency for energy system modeling. *Scientific data*, *6*(1), 1–10. doi: https://doi.org/10.1038/s41597-019-0199-y

Sanaieian, H., Tenpierik, M., Van Den Linden, K., Seraj, F. M., & Shemrani, S. M. M. (2014). Review of the impact of urban block form on thermal performance, solar access and ventilation. *Renewable and Sustainable Energy Reviews*, *38*, 551–560. doi: https://doi.org/10.1016/j.rser.2014.06.007

Santin, O. G., Itard, L., & Visscher, H. (2009). The effect of occupancy and building characteristics on energy use for space and water heating in dutch residential stock. *Energy and buildings*, *41*(11), 1223–1232. doi: https://doi.org/10.1016/j.enbuild.2009.07.002

Segers, R., Niessink, R., Van Den Oever, R., & Menkveld, M. (2019). *Warmtemonitor 2017*. Petten: CBS TNO. Retrieved from `https://publications.tno.nl/publication/34637063/VUtytF/segers-2020-warmtemonitor.pdf`

Sifnaios, I., Jensen, A. R., Dannemand, M., & Dragsted, J. (2021). Demonstration of a domestic photovoltaic-thermal (pvt)-heat pump system, performance simulation, and economic analysis for different climates. In *Swc 2021: Ises solar world congress* (pp. 588–599). doi: https://doi.org/10.18086/swc.2021.26.03

Statistics Netherlands CBS. (2022a). *Electricity balance sheet; supply and consumption.* Retrieved from `https://opendata.cbs.nl/#/CBS/en/dataset/84575ENG/table?dl=63D54` (Retrieved on 2-10-2023)

Statistics Netherlands CBS. (2022b). *Energy consumption private dwellings; type of dwelling.* Retrieved from `https://opendata.cbs.nl/#/CBS/en/dataset/81528ENG/table` (Retrieved on 29-9-2023)

Statistics Netherlands (CBS). (2022). *Solar power, assets for businesses and homes.* Retrieved 2023-09-29, from `https://opendata.cbs.nl/#/CBS/nl/dataset/85005NED/table`

Swan, L. G., & Ugursal, V. I. (2009). Modeling of end-use energy consumption in the residential sector: A review of modeling techniques. *Renewable and sustainable energy reviews*, *13*(8), 1819–1835. Retrieved from https://doi.org/10.1016/j.rser.2008.09.033

Ul-Abdin, Z., Zeman, M., Isabella, O., & Santbergen, R. (2024). Investigating the annual performance of air-based collectors and novel bi-fluid based pv-thermal system. *Solar Energy*, *276*, 112687.

van Rossum, A. (2024). Developing and implementing toolbox integrations for storing excess heat generated by a pvt system. Retrieved from http://resolver.tudelft.nl/uuid:b4066b14-7087-4ab7-8628-e7a2af4a2b83

Vogt, M., Tobon, C. R., Alcaniz, A., Procel, P., Blom, Y., El Din, A. N., ... others (2022). Introducing a comprehensive physics-based modelling framework for tandem and other pv systems. *Solar Energy Materials and Solar Cells*, *247*, 111944. doi: https://doi.org/10.1016/j.solmat.2022.111944

Wiedenhofer, D., Lenzen, M., & Steinberger, J. K. (2013). Energy requirements of consumption: Urban form, climatic and socio-economic factors, rebounds and their policy implications. *Energy policy*, *63*, 696–707. doi: https://doi.org/10.1016/j.enpol.2013.07.035

Williams, C. J., Binder, J. O., & Kelm, T. (2012). Demand side management through heat pumps, thermal storage and battery storage to increase local self-consumption and grid compatibility of pv systems. In *2012 3rd ieee pes innovative smart grid technologies europe (isgt europe)* (pp. 1–6). doi: https://doi.org/10.1109/ISGTEurope.2012.6465874

Yıldız, A., & Yıldırım, R. (2021). Investigation of using r134a, r1234yf and r513a as refrigerant in a heat pump. *International Journal of Environmental Science and Technology*, *18*(5), 1201–1210. doi: https://doi.org/10.1016/j.ijrefrig.2017.02.005

York, R. (2007). Demographic trends and energy consumption in european union nations, 1960–2025. *Social science research*, *36*(3), 855–872. doi: https://doi.org/10.1016/j.ssresearch.2006.06.007

Appendix A

Appendix

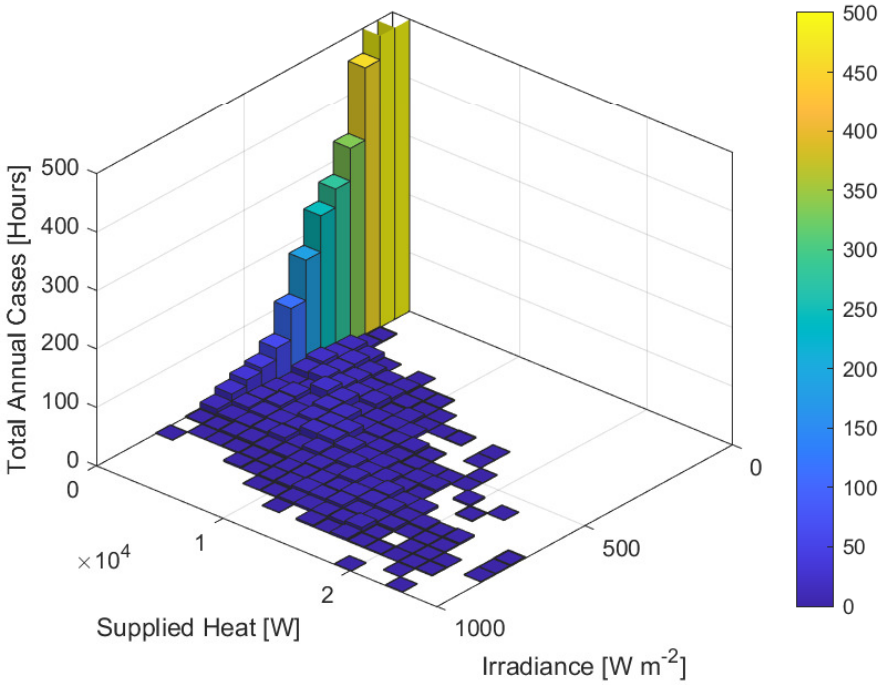

Figure A.1: Histogram of the operational HP conditions of summer mode.

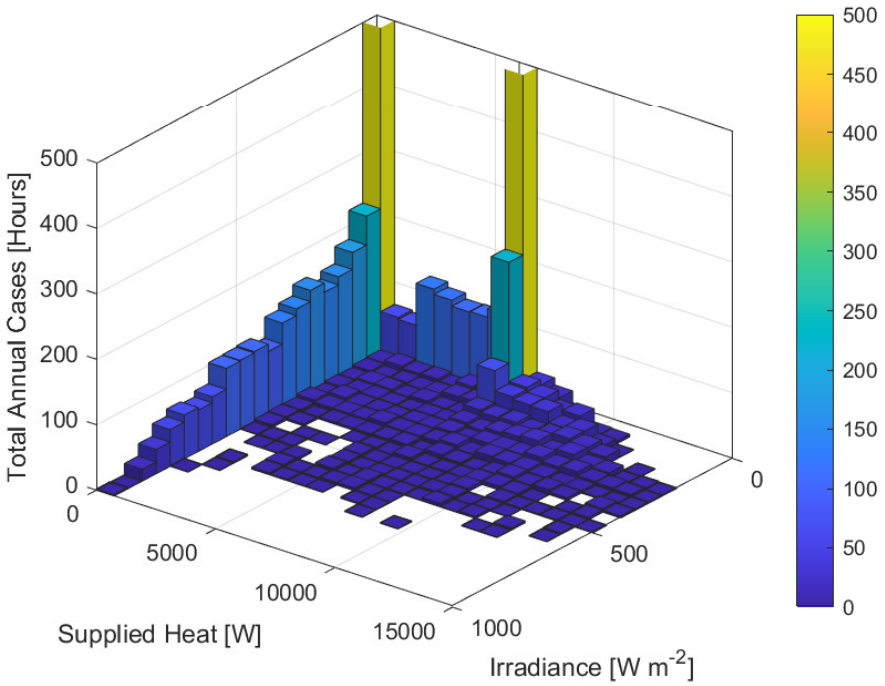

Figure A.2: Histogram of the operational HP conditions of spring mode.

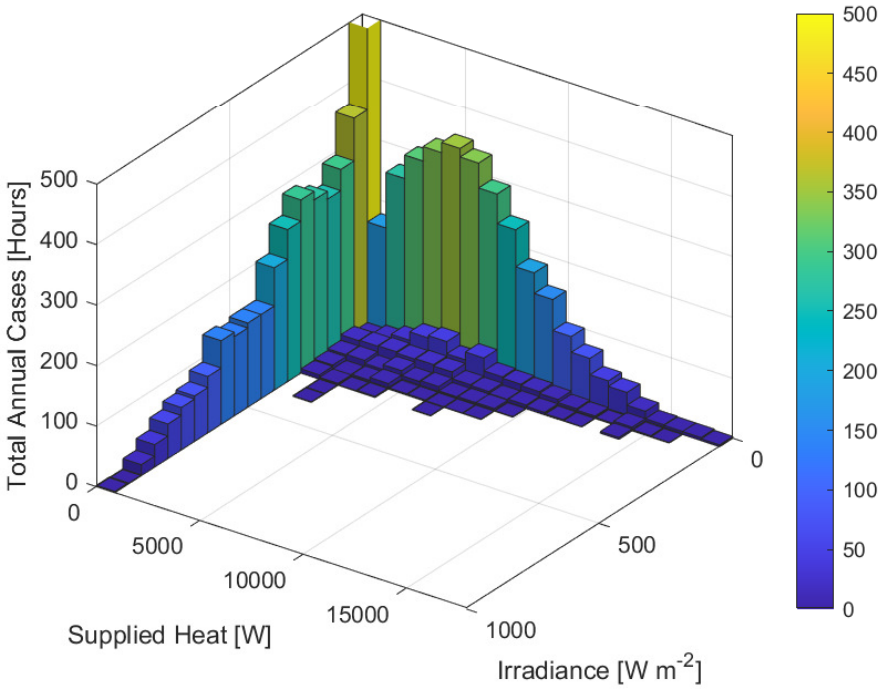

Figure A.3: Histogram of the operational HP conditions of winter mode.